



ACADÉMIE
DES SCIENCES
INSTITUT DE FRANCE

Comptes Rendus

Géoscience

Sciences de la Planète

Olivier Lacombe and Nicolas Emmanuel Beaudoin

Timing, sequence, duration and rate of deformation in fold-and-thrust belts: a review of traditional approaches and recent advances from absolute dating (K–Ar illite/U–Pb calcite) of brittle structures


Volume 356, Special Issue S2 (2024), p. 467-494

Online since: 31 May 2023

Part of Special Issue: Geodynamics of Continents and Oceans – A tribute to Jean Aubouin

Guest editors: Olivier Fabbri (Université de Franche-Comté, UMR CNRS 6249, Besançon), Michel Faure (Université d'Orléans-BRGM, UMR CNRS 7325, Institut des Sciences de la Terre, Orléans), Jacky Ferrière (Université de Lille, faculté des Sciences), Laurent Jolivet (Sorbonne Université, IStEP, UMR 7193, Paris) and Sylvie Leroy (Sorbonne Université, CNRS-INSU, IStEP, Paris)

<https://doi.org/10.5802/crgeos.218>

 This article is licensed under the
CREATIVE COMMONS ATTRIBUTION 4.0 INTERNATIONAL LICENSE.
<http://creativecommons.org/licenses/by/4.0/>



*The Comptes Rendus. Géoscience — Sciences de la Planète are a member of the
Mersenne Center for open scientific publishing*

www.centre-mersenne.org — e-ISSN : 1778-7025

Research article

Geodynamics of Continents and Oceans – A tribute to Jean Aubouin

Timing, sequence, duration and rate of deformation in fold-and-thrust belts: a review of traditional approaches and recent advances from absolute dating (K–Ar illite/U–Pb calcite) of brittle structures

Olivier Lacombe^{Ⓜ,*,a} and Nicolas Emmanuel Beaudoin^{Ⓜ,b}

^a Sorbonne Université, CNRS-INSU, Institut des Sciences de la Terre de Paris - ISTeP, Paris, France

^b Université de Pau et des Pays de l'Adour, E2S UPPA, LFCR, CNRS, TotalEnergies, Pau, France

E-mails: olivier.lacombe@sorbonne-universite.fr (O. Lacombe), nicolas.beaudoin@univ-pau.fr (N. E. Beaudoin)

Abstract. Based on a review of literature and a few case studies, this paper summarizes the state of the art on the dating of folds and thrusts, then presents and discusses how recent advances in K–Ar illite and U–Pb calcite geochronology applied to brittle structures in fold-and-thrust belts have helped better constrain the timing, sequence, duration and rates of deformation.

Keywords. Fold-and-thrust belt, Geochronology, Folds, Thrusts, Timing, Duration and rate of deformation.

1. Introduction

Fold-and-thrust belts (FTBs hereinafter) are important features of almost all modern convergent orogens. FTBs mark the boundary between the orogen (hinterland) and its foreland basin and correspond to the zone of frontal tectonic accretion of shallow crustal rocks (Figure 1A). In FTBs, the migration of deformation through time in response to the growth of the orogenic wedge usually involves the proximal parts of the foreland basin and causes folding of the pre-orogenic and syn-flexural sedimentary sequences. In most cases, sedimentation occurs continuously during deformation and growth strata are

deposited synchronously with folding on top of pre-folding strata.

In order to understand the rates and mechanisms of orogenic growth, it is important to determine the age and longevity of structures such as folds and thrusts. Such chronologic constraints are critical for defining the timing, duration and rate of shortening, fold growth and deposition [Suppe et al., 1992, Butler and Lickorish, 1997] and more generally the sequence of deformation. In FTBs, the general case is a foreland younging sequence of thrusts and related folds (“in-sequence” thrusts), but thrusts can also violate this trend (“out-of-sequence” thrusts), and the sequence may even be erratic in case of strong structural inheritance. In order to reconstruct the tectonic evolution, it is therefore critical to determine the ages and duration of the involved folds and thrusts as well as the associated local and regional deformation

*Corresponding author

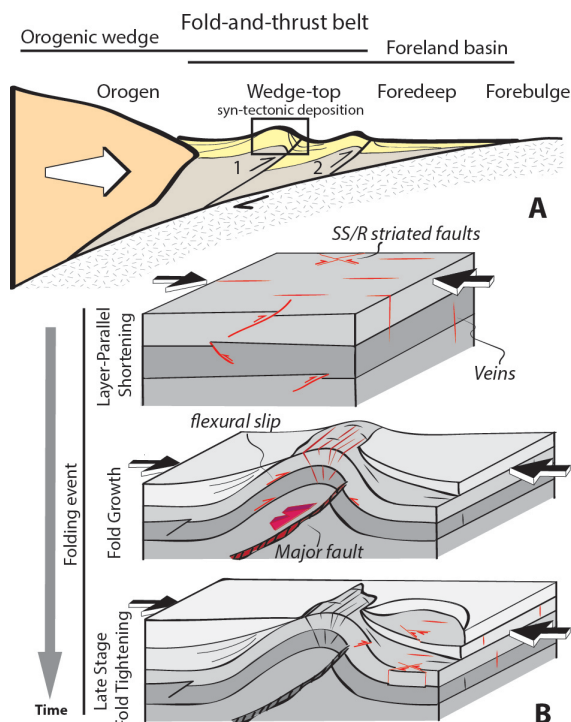


Figure 1. (A) Definition of the various domains of the fold-and-thrust belt-foreland basin system. (B) Sketches of the 3 deformation stages defining the folding event, on which developing structures used for dating deformation are represented in red.

rates.

The age of shallow-crustal thrusts and folds is usually constrained either by indirect bracketing, relying on the age of the formations that are thrust and/or folded and of those sealing the thrust or the fold, or by direct dating of syn-orogenic sedimentation. Efforts have been made to provide age constraints on the deposition of growth strata or on uplifted/deformed fluvial or marine terraces. However, in addition to the uncertainties inherent to stratigraphic correlation, this approach is obviously limited where no record of syn-orogenic sedimentation is preserved. It is therefore of prime interest to directly date either folding or faulting whenever possible. The absolute age of activity for shallow-crustal faults can be obtained by geochronology of fault-generated materials such as fault gouge, slip-surface hematite or opal, pseudotachylyte and slick-

enfibers [e.g., Nuriel et al., 2012, 2019, Ault et al., 2015, Tillberg et al., 2020]. More common minerals suitable for radiometric dating include the K-bearing illite [van der Pluijm et al., 2001, Vrolijk et al., 2018] or the U-bearing calcite [Roberts and Walker, 2016, Roberts et al., 2017].

Direct dating of folding requires preliminary identification of datable mineral-bearing mesostructures (e.g., calcite-filling veins or slickensides/calcite steps along faults or bedding-parallel slip surfaces) that developed contemporaneously with folding. For a given contractional event leading to folding, mesoscale structures may form before, during and after folding, i.e., in a sequence than encompasses layer-parallel shortening (LPS), fold growth and late stage fold tightening (LSFT) [Tavani et al., 2015; Figure 1B]. This sequence defines the folding event [Lacombe et al., 2021]. The identification and absolute dating of early-, syn- and late-folding mesostructures provides a time bracket for fold growth and allows for an unprecedented assessment of the timing and duration of fold-related contraction.

Because a wealth of absolute dates have been gained from various techniques over the last 15 years in contractional settings worldwide, it is timely to review the classical approaches and recent advances on dating folding and thrusting in FTBs, and to show how geochronology may help better constrain the sequence, duration and rates of shortening and propagation of deformation. We first provide a brief review of the classical approaches to date fold growth and to constrain folding rates. Second, by focusing on brittle deformation, we show (1) how direct dating of illite from fault gouges provides first-order information of the timing of thrusting, and (2) how direct dating of calcite mineralization associated with the development of mesostructures within folded strata help constrain the timing and duration of folding and/or of shortening preceding and following folding. We finally discuss how geochronology has paved the way toward a better appraisal of the sequence and rates of deformation in FTBs.

2. Dating fold growth using the sedimentological record

2.1. Growth strata

Over timescales of 100 kyr to My, the timing and rate of fold development can be obtained from syn-

orogenic formations if they are preserved and datable. Syn-folding growth strata depositing on top of pre-folding strata often show a first-order characteristic pattern: decreasing dips up section toward the fold flanks; fan-like geometry, with thickening of beds away from the fold limb/crest; conformable bedding except at the edges of the fold where unconformities are observed along with tapering bed thicknesses (Figure 2A). Syn-tectonic unconformities may be either progressive or angular, respectively resulting from either slow or rapid tilting of the depositional surface with respect to sedimentation rate [Riba, 1976]. The transition from conformable beds to unconformities is usually interpreted as representing a change from stable to tectonically active conditions where the fold may begin to emerge above the land surface [Poblet et al., 1997]. Because of the competition between sedimentation and fold uplift which may vary over time, growth strata may exhibit variable geometries: onlap, offlap, overlap, with variable or constant thickness. For instance, growth beds that overlap the fold crest and thin over it indicate that sedimentation rates outpaced fold growth rates during their deposition; overlapping beds with constant thickness indicate that no fold uplift occurred during their deposition. Growth strata are variably preserved in the sedimentary record depending on the amount and rate of erosion [Vergés et al., 2002]. The geometries and sedimentological characteristics (e.g., changes in vertical facies succession and provenance) of growth strata associated with a given fold are key to understanding its kinematics. Several factors such as axial surface activity, fold uplift, limb rotation and limb lengthening rates, deformation mechanisms within the syntectonic sediments, together with sedimentation and erosion rates, control growth strata patterns. Because the evolutionary path of most of these parameters depends on the fold kinematics, different growth strata architectures are expected for different thrust-related folds [Suppe et al., 1992]. Growth strata have been extensively documented [e.g. Lickorish and Ford, 1998, Butler and Lickorish, 1997, Schneider et al., 1996, Zapata and Allmendinger, 1996, Saura et al., 2011, Heermance et al., 2008, Chen et al., 2022]. Dating the base of the growth strata defines the youngest initiation age for fold growth, while the end of folding is marked by deposition of post-growth strata concealing the final fold geometry. As a result, it is of the utmost

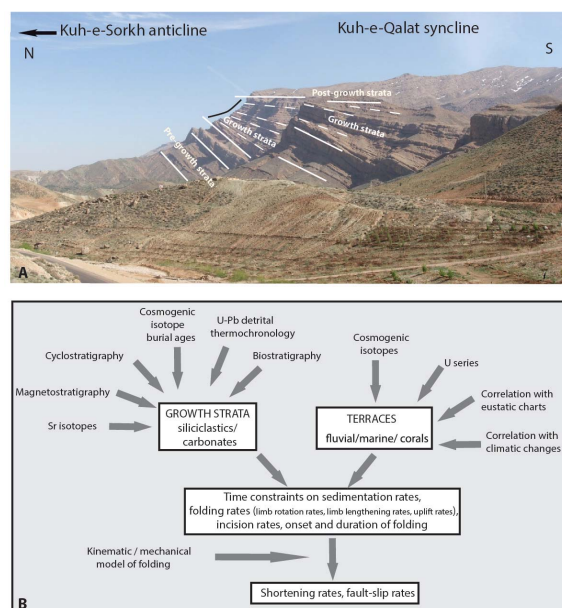


Figure 2. (A) Photograph of growth strata (Fars, Iran). (B) Summary of dating techniques applied to growth strata and terraces and usual workflow to estimate shortening or fault-slip rates.

importance to provide absolute age constraints on growth strata deposition, with the currently available techniques to do so being summarized hereinafter (Figure 2B).

2.1.1. *Magnetostratigraphy*

Magnetostratigraphy relies upon collecting samples from fine-grained lithotypes along a stratigraphic section and analyzing them to determine their characteristic depositional remanent magnetization (ChRM). The ChRM direction usually represents a primary magnetization acquired at, or shortly after, rock deposition and is used for the calculation of the Virtual Geomagnetic Pole (VGP) latitude at each stratigraphic level. Positive and negative VGP latitudes are interpreted as normal and reverse polarity, respectively, and used to construct a local magnetic polarity stratigraphy of the section. When combined with independent anchor absolute ages, the local magnetostratigraphic column is correlated with the Global Magnetic Polarity Time Scale, which ultimately yields the absolute age of the stratigraphic section, including the growth strata of interest. The

main issue is related to variations in the deposition rate, which can cause the thickness of a given polarity zone to vary from one area to another. This technique is well suited to date non marine sequences that generally lack fossiliferous contents.

2.1.2. *Biostratigraphy and strontium isotopes*

In the case of carbonates, time constraints on the age of growth strata come from either classical biostratigraphy or strontium isotope stratigraphy. The latter method relies on the comparison of the Sr isotope ratio $\text{Sr}^{87}/\text{Sr}^{86}$ of the samples with the reference curve documenting the evolution of the value of the $\text{Sr}^{87}/\text{Sr}^{86}$ ratio of the ocean through geological time [McArthur et al., 2012] to derive the age of the sample.

2.1.3. *U–Pb detrital thermochronology*

Dating of detrital zircons from clastic sedimentary rocks provides information about provenance, hence source areas. The dating of the detrital component of growth strata allows the analysis of the different source areas through time, which in turn would indicate successive uplift and exhumation of the recognized morphostructural systems. U–Pb detrital thermochronology also may provide direct chronostratigraphic information on the growth strata of interest. DeCelles et al. [2007] reported the study of clastic sedimentary rocks in the Puna plateau (Argentina) where, in addition to older zircon grain populations, the age of a small population of detrital zircon ages overlaps with biostratigraphic ages and helped refine the stratigraphic age of the formation.

2.1.4. *Pairing $^{26}\text{Al}/^{10}\text{Be}$ burial dating and magnetostratigraphy*

Because magnetostratigraphic dating fails in coarse-grained growth strata and in areas with few interbedded volcanic layers and sparse biostratigraphy, burial dating has emerged as a new way to date such strata in late Cenozoic basins. Thompson Jobe et al. [2018] combined magnetostratigraphy with $^{26}\text{Al}/^{10}\text{Be}$ cosmogenic burial age dating in growth strata of the Tarim Basin to place age constraints on depositional sequences and to define fold initiation. Burial ages are most reliable when derived from slowly eroding source terranes that have been (1) deeply and rapidly buried, and (2) only very recently exhumed.

2.1.5. *Cyclostratigraphy*

Sedimentary rocks often record Milankovitch-scale cyclicity, which can be revealed by rock-magnetic methods. Cyclostratigraphic records related to magnetic-mineral concentration variations modulated by astronomically forced climate changes can be used to date growth strata [e.g., Carrigan et al., 2016]. Cyclostratigraphy provides temporal resolution on the order of 10^4 – 10^5 years in clastic and carbonate marine [Hinnov, 2013] and fluvial [Nádor et al., 2003] deposits. Foreland basins are well suited for cyclostratigraphy as they have sufficiently high sediment accumulation rates and large accommodation space to record high frequency orbital signals.

2.2. *Terraces*

Fold geometry and short term rates of deformation over a timescale of ~ 10 kyr can be determined using geomorphic studies of uplifted terraces and dated terrace fill or strath surfaces across active structures [Delcaillau, 2001]. Nearly isochronous fluvial or marine terraces can be used as geomorphic strain markers linking underlying structures to surface deformation, in order to deconvolve the shortening and uplift of a fold. Fluvial terraces provide important records of river incision, rock uplift, and climatic perturbations [e.g. Pazzaglia and Brandon, 2001]. Remnants of warped and tilted fluvial terraces preserved along rivers in active orogens reflect the long-term incision history of a river and can be used as geomorphic markers to interpret active folding, provided the river profile does not change through time [e.g. Lavé and Avouac, 2000]. If the age of the terraces can be assessed, fluvial terraces provide information on rock uplift rates (and on folding rates if rock uplift is related to folding). Marine terraces can also be used to unravel vertical deformation. In contrast to fluvial terraces, their initial elevation and geometry are usually affected by less ambiguity and provide a more accurate tectonic signal, although their restricted areal extension limits their use to the shorelines of coastal orogens.

The derivation of rock uplift rate from dated fluvial terraces requires that the geometry and elevation of the river remain constant during incision. Rock uplift is equal to river incision, as measured from

the elevation of terrace remnants above the modern river channel. However, a river can also incise due to climatically-induced channel geometry and base level changes, so that local incision does not necessarily equal local tectonic uplift. It is generally considered that fluvial terraces forming a level at a continuously varying elevation above the modern river bed are isochronous [e.g., Molnar et al., 1994].

Terraces may be laterally correlated according to the thickness, grain size and degree of weathering of their fill. The age of the terraces can be assessed using different methods such as ^{14}C dating of organic-carbon rich material in the terraces, minimum exposure ages determined from in situ produced cosmogenic radionuclides (^{10}Be , ^{36}Cl) on pebbles and clasts from the terrace surfaces [Cerling and Craig, 1994, Gosse and Phillips, 2001] or luminescence of feldspar or quartz [Rizza et al., 2019]. Terrace exposure ages correspond to the time since terrace abandonment, when fluvial incision resumed.

Finally, uplifted quaternary coral reef terraces (constructional or erosional) have also been used to derive rate of late Quaternary folding [Taylor and Mann, 1991, Cox, 2009].

2.3. *From depositional patterns and age of growth strata and terraces to fold growth rate and from fold growth rate to shortening rate*

Depositional patterns and ages of growth strata allows to constrain how and how fast fold attributes (fold uplift, limb rotation) have been progressively acquired through time. The crestal structural relief of a fold can be defined as the elevation of a given stratigraphic horizon in the anticline crest with respect to the same horizon off the fold [McClay, 1992]. Knowing the crestal structural relief at different times makes it possible to estimate the fold uplift during deposition of a particular growth bed as well as fold uplift rates if beds can be dated [Masferro et al., 2002]. Kinematic models of fault-related folding consistent with the pattern of growth strata can subsequently be used to derive shortening rates and fault-slip rates (Figure 2B).

The Zagros belt case illustrates how the timing, regional in-sequence fold development and rates of fold/thrust propagation have been constrained using magnetostratigraphy [Khadivi et al., 2010, Ruh et al., 2014, Pirouz et al., 2017, Najafi et al., 2021].

Also, the duration of some fold growth was constrained thanks to the dating of both the base and top of the growth strata [Changuleh syncline: 5 Myr, Homke et al., 2004; Jarik syncline: 5.8 Myr, Lashgari et al., 2020; Dowlatabad syncline: 2.85 Myr, Najafi et al., 2021]. The mean rates of folding front propagation (20 mm/yr in the Fars and 15 mm/yr in the Lurestan, varying with time between 8 and 34 mm/yr) are about one order of magnitude larger than the coeval shortening rates (~ 4 mm/yr in the Fars and ~ 2 mm/yr in the Lurestan). The fast propagation is possibly related to either the reactivation of pre-existing faults in the Arabian basement or the presence of an efficient decollement at the base of the deformed Arabian sedimentary cover (Hormuz evaporites).

Uplifted and tilted fluvial or marine terraces also can be used to reconstruct the pattern of vertical movements related to folding. Terrace ages can be combined with estimated terrace uplift and terrace height profiles to evaluate the average uplift rates. Considering a fold model accounting for the pattern of uplift rates allows for conversion of the (vertical) uplift rate into an (horizontal) shortening rate. For instance, Lavé and Avouac [2000] used a fault bend fold model to estimate the shortening rates associated with folding in the Himalaya foreland. The rock uplift rate of up to 1.5 cm/yr derived from river incision was converted into a mean shortening rate of 21 ± 1.5 mm/yr over the Holocene, which indicates that thrusting along the Main Frontal Thrust accommodates most of the shortening rate across the whole Himalaya. More applications can be found in the literature [e.g., Thompson et al., 2002, Simoes et al., 2007, Haghipour et al., 2012, Hu et al., 2017]. Rockwell et al. [1988] investigated the late Quaternary fluvial terraces uplifted and folded over the Ventura Avenue anticline (California) and showed that the minimum possible average uplift rate in the axial region of the fold has decreased from ~ 14 mm/yr to 2 mm/yr during the past 200 ka. Interval uplift rates for the periods ~ 200 –100 ka, ~ 100 –30 ka and 30 ka-present are, respectively, about 20 mm/yr, 9 mm/yr, and 5 mm/yr. Based on the mechanics of flexural slip folding, these data indicate a relatively constant shortening rate of ~ 9 mm/yr since the fold inception. Interestingly, a constant shortening rate can produce systematic changes of the rate of uplift and tilting over time as a result of local time-dependent fold mechanics.

To sum up, short-term and long-term shortening rates can significantly differ, and variable short-term fold uplift rates may be consistent with a constant shortening rate. Average deposition and fold growth rates are often derived by assuming a steady shortening rate. Assuming both rates were constant throughout the fold history, a tentative time of fold inception can be assessed. However, fold growth has a highly discontinuous character through time, with deformation being episodic at all timescales with tectonic uplift pulses of different duration and intensity interrupted by periods of variable extent in which no fold growth occurred [e.g., Masferro et al., 2002, Livio et al., 2007, Anastasio et al., 2017]. The growth of some fault-related folds may be related to earthquake-related slip on active faults, which is by essence discontinuous. Recent studies combining magnetostratigraphy and cyclostratigraphy suggest highly variable deformation rates [Carrigan et al., 2016]. This emphasizes the difficulty to extrapolate back in time the short-term fold uplift and shortening rates, and questions the true meaning of average fold uplift rates. The age of fold initiation obtained by assuming steady shortening, deposition, and fold growth/uplift rates is therefore at best strongly biased and at worst false, so the duration of fold growth remains poorly constrained.

3. Dating thrust timing and quantifying slip rates using low- T thermochronology coupled with thermal-kinematic-thermochronometric modeling

Low- T thermochronological techniques such as fission tracks or (U-Th)/He dating of apatite have the potential to resolve the timing of activity of thrusts and related slip rates averaged over long timescales in FTBs. That is done by deriving cooling ages recording erosion associated with the activity of the structures. Low- T thermochronology also has been used to constrain the age of initiation of a thrust belt and/or the timing of individual thrust sheets by identifying “steps” in the cooling age across thrust sheets [e.g., Arne et al., 1997, Viola et al., 2003, McQuarrie et al., 2005, Sobel et al., 2006]. Lock and Willett [2008] proposed a systematic study of the patterns of low- T thermochronometric ages generated in material exhumed by thrust-driven erosion across a FTB encompassing a complex series of faults. They also in-

vestigated how these patterns change with fault geometry and thrusting rate. The comparison of the cooling age patterns associated with individual and multiple thrusts derived from thermal-kinematic-thermochronometric modeling with natural cooling age patterns provides a tool to help quantify and interpret the amount, timing and rates of thrust-related deformation.

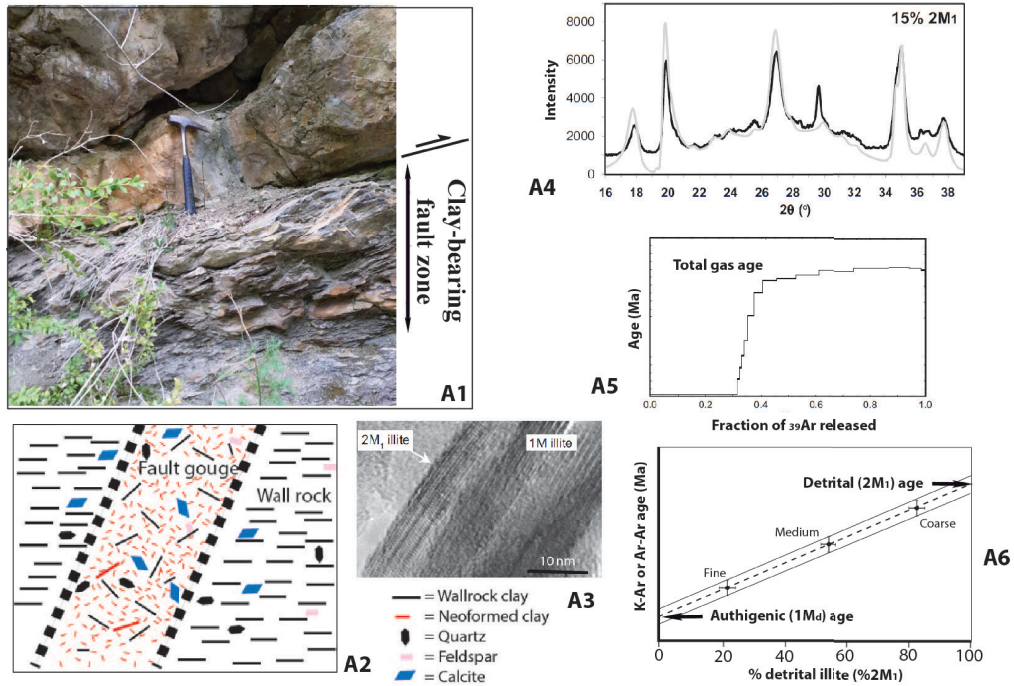
4. Recent progress in using geochronology for dating thrusts and folds (1): K-Ar and Ar-Ar geochronology of syn-kinematic authigenic illite

4.1. Principle of the technique (Figure 3A)

The clay fraction of clay-rich rocks is composed of a mixture of clays with multiple origins (detrital and authigenic). In low-grade shales and mudstones, the detrital mica component is characterized by 2M1 polytype, whereas the authigenic form is the 1M/1Md polytype (typically mixed-layer illite-smectite (I-S) [Velde and Hower, 1963, Clauer et al., 1997, Srodon et al., 2002]. 2M1 mica-discrete illite is considered to be the detrital phase because its crystallization temperature exceeds 280 °C [Srodon and Eberl, 1984]. In contrast, the 1Md polytype is thought to form at significantly lower temperatures (T) below 200 °C during diagenesis [Velde, 1965]. The finer (<1 μ m) fractions of shales tend to be more enriched in authigenic mixed-layer illite-smectite than coarser fractions.

A fault gouge forms by a combined process of mechanical comminution and in situ neocrystallization of phyllosilicates during fluid-assisted faulting. Dating of a fault gouge relies upon textural arguments to deduce that the formation of the gouge is associated with instantaneous neoformation of illite that is related to strain rate in the fault zone (i.e. more neoformation during higher shear strain rate), because the energetics of faulting and fluid flow promotes growth of authigenic illite. Illite can form by illitization of fragmented smectite [Altaner and Ylagan, 1997], by hydration reactions of mica or by neocrystallization from a fluid phase [Mancktelow et al., 2015], and possibly by breakdown of K-feldspar [Zwingmann et al., 2010]. Thus, K-Ar or Ar-Ar isotopic dating of illites in fault gouge provides a powerful tool to directly date fault slip.

A. K-Ar or Ar-Ar dating of illite-bearing fault gouge



B. LA-ICP-MS U-Pb dating of calcite cement from veins or slip surfaces

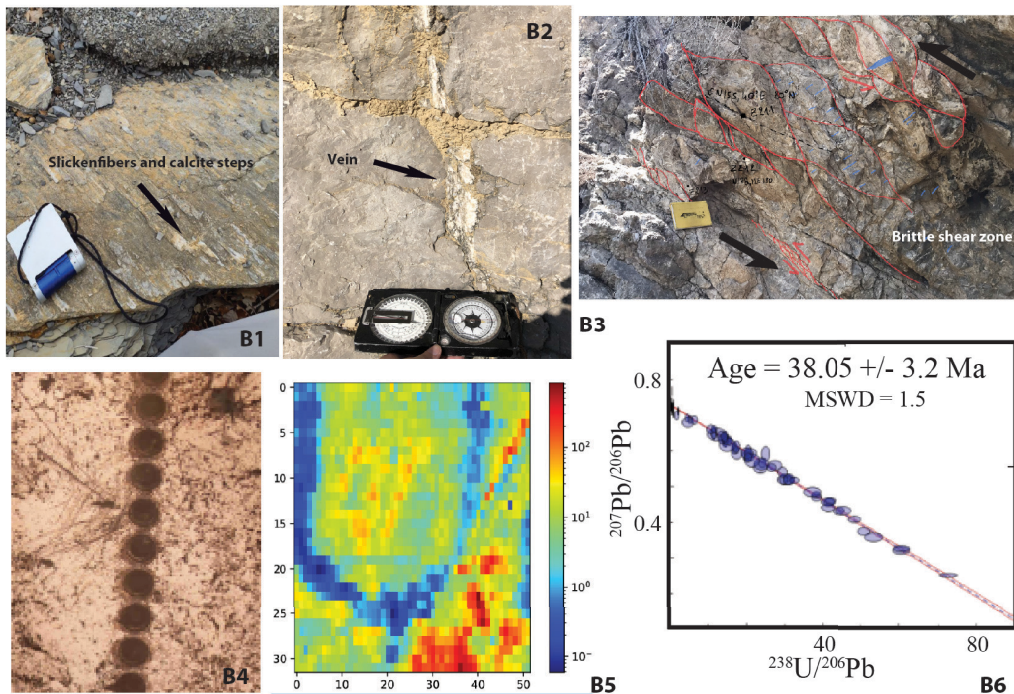


Figure 3. Caption continued on next page.

Figure 3. (cont.) (A) K–Ar/Ar–Ar illite geochronology. A1: example of clay-bearing thrust fault zone; A2: schematic fault gouge with wall-rock derived clay and authigenic clay [after Haines and van der Pluijm, 2023]; A3: electron microscope image of 2M1 and 1M illite assemblage; A4: polytype quantification using XRD: fit of sample size fraction pattern and synthetic pattern of a mixture of 2M1 and 1Md illite; A5: Ar-degassing age spectra; A6: plot of % 2M1 illite versus age of size fractions. (B) U–Pb calcite geochronology. Examples of dated mesostructures (B1: calcite steps along a flexural slip surface; B2: tectonic vein; B3: calcite along slip surfaces in a brittle shear zone). Principle of dating of syn-kinematic calcite mineralization using LA-ICP-MS (B4: laser ablation spots in a calcite vein; B5: map of the $^{238}\text{U}/^{207}\text{Pb}$ ratio within a calcite step; B6: Tera–Wasserburg diagram).

However, shallow crustal fault gouges as encountered in FTBs consist in a mixture of low T , authigenic 1M/1Md illite generated by fault activity and of a higher T , detrital 2M1 illite derived from cataclasis of wall rocks during slip (note that in high T fault gouges, 2M1 also forms as a syn-kinematic/authigenic polytype). The physical mixing between the inherited host rock fragments and the authigenic phases formed during faulting is a challenge when interpreting K–Ar illite results from brittle fault rocks, as it is necessary to discriminate the radiogenic isotopic signature of both components. Unfortunately, the lower the shear strain rate and the temperature, the greater this challenge, because of the only partial isotopic resetting of the inherited components and limited authigenesis. Careful sample characterization and data reduction and analysis from multiple grain size fractions are thus necessary to produce dates that are not spurious due to mixed radiogenic signatures.

As the growth kinetics of large clay crystallites at low T is unfavorable, authigenic clays in shallow crustal fault gouges are typically very fine-grained ($<1\ \mu\text{m}$) and thus tend to preferentially concentrate in the finest size fraction. The age of the finer ($<0.1\ \mu\text{m}$) illite fraction is likely to be the closest to the latest episode of faulting recorded by the fault rock through the growth of syn-kinematic authigenic illite. In contrast, the age of the coarsest fractions represents a protolithic component, i.e., an inherited input to the fault rock derived from the host rock [Viola et al., 2016]. However, although the finest fraction is expected to provide the closest age to the age of authigenic mineralization and, thus, to faulting [Age Attractor Model, Torgersen et al., 2015b], it still generally contains some detrital material, and therefore the age of that fraction will be a mixing age. The ability to extract geologically meaningful neoforma-

tion ages from clay-rich fault rocks therefore requires careful characterization of the clay populations and the accurate quantification of the amounts of detrital and authigenic phases.

The first step of the dating procedure consists in characterizing the relative abundances of the authigenic 1Md polytype and the cataclastically-derived 2M1 polytype of illite in several (3 at least) size fractions of the fault gouge. After separation of the different size fractions (coarse: 2–even up to 6–10- μm –0.2 μm ; medium: 0.2 μm –0.05 μm ; fine: $<0.05\ \mu\text{m}$), the amounts of detrital and authigenic illite are quantified in each fraction by measuring the amounts of discrete illite and interlayered illite–smectite (I–S) [van der Pluijm et al., 2001]. The authigenic/detrital ratio is determined through X-ray analysis of the clay fraction. Illite polytypism can alternatively be quantified by modeling X-ray powder diffraction patterns [Reynolds, 1993]. The percentage of detrital illite in each size fraction can be established by matching the sample XRD pattern with synthetic XRD patterns of mixed 2M1 and 1Md components [Haines and van der Pluijm, 2023]. It is also possible to determine the concentration of the 2M1 polytype by measuring the area of peaks that are unique to the 2M1 polytype and finding the ratio of them against the area of a peak which is common to both polytypes [Grathoff and Moore, 1996, Solum and van der Pluijm, 2007, Aldega et al., 2019]. In a second step, the different size fractions of the gouge are dated using $^{40}\text{K}/^{40}\text{Ar}$ or $^{40}\text{Ar}/^{39}\text{Ar}$ methods [Clauer et al., 2012]. If samples consist of different mixtures between the two polytypes, and assuming a two-end member mixing model, the radiogenic $^{40}\text{Ar}/\text{K}$ ratio of each mixture (i.e., each different clay size fraction) that contain different relative percentages of each clay polytype should fall on a binary mixing line between the two end-member ratios. A fitted line through

the data points of a fault rock samples with multiple grain-size fractions containing various percentages of detrital clay can therefore be extrapolated to 0% detrital illite to obtain an estimate for the age of the pure authigenic component [Illite Age Analysis, Pevear, 1999].

For further details, the reader is referred to the papers by Clauer [2013], Viola et al. [2016], Boles et al. [2018], Vrolijk et al. [2018] and Song and Sim [2021].

4.2. *Limitations and way forward*

Fault ages calculated using the two-end member mixing model correspond to discrete events that represent either the timing of short-lived faulting or a finite period of fault slip in the presence of fluids [Haines and van der Pluijm, 2008, Solum et al., 2005, van der Pluijm et al., 2006]. Therefore, capturing the entire history of fault activity from a single fault-gouge age remains challenging and unlikely. The potential for wall rock inheritance and multiple clay-generating slip events generally results in a positive correlation between K–Ar illite age and clay grain size [e.g., Torgersen et al., 2015a,b], which can be challenging to deconvolve.

The conditions under which authigenic clay forms in a fault zone are critical to the interpretation of illite ages. One can wonder how reliably the obtained age of authigenic illite can be interpreted in terms of the fault-zone development, particularly within the framework of thermo-tectonic evolution.

Temperature is likely to be one of the key parameters controlling its growth. The potential temperature control on illite growth has implications for the interpretation of authigenic illite ages and their relationship to deformation episodes within fault zones [Duvall et al., 2011]. Zwingmann and Mancktelow [2004] proposed that illite grows at temperatures in the range 120 °C–150 °C. The range of temperature for 1Md authigenic illite formation has been assessed by Haines and van der Pluijm [2008] between 110 °C and 160 °C. For Duvall et al. [2011], the growth of authigenic illite is rather restricted to a narrow thermal window, 108 ± 10 °C. On the one hand, the K–Ar age of authigenic illite records the time elapsed since its in-situ mineralization within the fault zone. Any increase in temperature related to any secondary heating episode up to the closure temperature of illite K–Ar empirically estimated as

260 °C for a grain size of ~ 2 μm [Hunziker et al., 1986] will cause the opening of the illite K–Ar system [Tagami, 2012]. On the other hand, if the temperature window of authigenic illite growth is relatively narrow, then the range of fault depths where illite formation can occur is also limited, which allows for targeted sampling of clay gouges that correspond to particular periods of fault motion if the exhumation history of sample sites is known. However, capturing the record of the entire fault activity implies that fault slip occurred within the illite crystallisation temperature window and that the corresponding fault rocks are available for surface sampling. In addition, one can wonder about the possible formation of illite due to shear heating out of the expected geothermal temperature window [Rattez and Veveakis, 2020]. This means that the assumption that new authigenic illite growth occurs with each successive faulting event and completely overprints illite grown during the earlier phases of deformation—so that illite ages determined for faults with prolonged histories represent the last major period of fault slip [Solum et al., 2005, Haines and van der Pluijm, 2008]—may be wrong. The fault-formed illite age therefore does not always represent the latest phase of fault slip if the rocks sampled at the surface did not deform in, or where not exhumed from, this temperature windows or equivalent depth range, so that the recorded event could well be the initiation of faulting. Along distinctively buried and/or exhumed fault segments, the record of the stage of faulting along a given fault may therefore vary among sampling sites depending on the thermal history. Hernández-Vergara et al. [2021] reported Eocene illite ages for folding and thrusting in the Chiapas FTB (Mexico), but noticed the nearly complete absence of illite formed during the Miocene Chiapanecan Orogeny. Most of their samples still contain smectite, which did not fully morph into illite upon diagenesis as illite only has grown on secondary foliation planes. This suggests that the samples were moderately buried, and that only the most deeply buried ones recorded the Eocene folding. Erosion during the Eocene and Miocene orogenies may have brought all samples to temperatures too low for illite generation during the Chiapanecan folding. It thus follows that considering the temperature/depth at the time of faulting or folding is of primary importance for the interpretation of illite ages. The comparison of thermal histories with gouge ages

from a single fault or multiple faults offers independent information on the timing of discrete fault events along specific structures. The determination of thermal histories from thermochronometers like apatite fission track (closure temperature $\sim 110^\circ\text{C}$) places important constraints on the interpretation of gouge ages.

The first ways of improvement for the dating of fault gouges using K–Ar illite geochronology is related to the better characterization of illite. The habit and morphology of illite crystallites can be determined by scanning or transmission electron microscopy to discriminate different illite populations. The actual process responsible for illite authigenesis often remains unclear. Illite may grow during slip localization, but pre- or post-deformational hydrothermal alteration [Viola et al., 2013], diagenesis [Lanson et al., 2002] or deep weathering [Fredin et al., 2017] may also contribute to the crystallization of K-bearing phases [Scheiber et al., 2019]. Stable isotope studies [Mancktelow et al., 2015] and the determination of illite crystallinity [Verdel et al., 2011] may help constrain the influence of specific processes on the authigenesis of illite. The second way is to very closely link illite age to the detailed architecture and chronology of structural development of the fault zone, in other words, to conduct microstructurally-constrained illite geochronology. Studies aiming at dating fault slip generally focus on syn-kinematic authigenic illite from the fault cores. Strain during fault reactivation is confined to the fault core due to strain localization leading to fault narrowing. The fault core is characterized by incohesive fault rocks, large amount of secondary clay mineral assemblages, and large age spreads in K–Ar age-versus-grain-size spectra. Considering the so-called Brittle Structural Facies, i.e., commonly tightly juxtaposed, although not coeval, deformed volumes of rock within a fault zone, characterized by a given fault rock type, texture, colour, composition, and age of formation [Tartaglia et al., 2020], has been a step forward in the investigation of the diachronic evolution of fault cores and the resolution of multiple slip events along long-lived faults.

Despite these improvements, it remains a difficult task to fully constrain the timing of fault initiation and to decipher the complex reactivation history of long-lived brittle fault cores [Scheiber et al., 2019]. Alternatively, provided that a carefully

microstructural characterization of damage zone samples is performed, narrow K–Ar age ranges and even age plateaus can be obtained, which can be interpreted as recording fault initiation. Samples from cohesive damage zones therefore have the potential to preserve structural and mineralogical characteristics from the earliest stages of fault zone activity, even if the fault core was subsequently repeatedly active through time [Scheiber et al., 2019]. Torgersen et al. [2022] showed that it is even possible to obtain geologically significant K–Ar ages from several generations of syn-kinematic authigenic illite within the same fault gouge if careful field sampling and structural characterization is combined with detailed mineralogical characterization, including illite crystallinity analysis.

Finally, attention must be paid to the nature of the protolith at the expense of which the gouge forms. In the case of low T gouge material formed at the expense of siliciclastic turbidites or pelites, the problem of contamination by K-bearing minerals derived from the host rock of even the finest illite fractions, where the amount of contaminant is expectedly the least, may be striking [Carboni et al., 2020, Viola et al., 2018, 2022].

5. Recent progress in using geochronology for dating thrusts and folds (2): U–Pb geochronology of syn-kinematic calcite

LA-ICP-MS has been applied to U-series dating [Egins et al., 2005], and successful applications of U–Th dating to striated fault planes have been reported [Nuriel et al., 2012]. However, the usually very low ^{230}Th concentration in carbonates severely hampers the applicability of LA-ICP-MS to U-series calcite geochronology [e.g., Lin et al., 2017], which is moreover restricted to ages younger than ~ 500 kyr [Andersen et al., 2008]. U–Pb calcite geochronology does not suffer this limitation and allows dating of syn-kinematic carbonate mineralization as old as 10^8 yrs. Because the U–Th dating method has large uncertainties and requires relatively high U contents compared to U–Pb, we focus hereinafter on U–Pb calcite geochronology which is more applicable in most settings. We exclude from this review the recent application of LA-ICP-MS to U–Pb dating of dolomite [Bar et al., 2021, Elisha et al., 2021].

5.1. Principle of the technique (Figure 3B)

In FTBs, tectonic veins are very often filled with calcite, and mesoscale slip surfaces are also often coated with calcite. Dating the calcite mineralization directly associated with fracturing or faulting [i.e., tectonic carbonates *sensu* Müller, 2003], may therefore provide valuable constraints on the timing of development of the set of structures the veins/faults belong to.

Polished sections of vein-filling calcite, cataclase-cementing calcite or fault plane-decorating calcite are analyzed by LA-ICP-MS using standard methods for calcite U–Pb geochronology [e.g., Roberts et al., 2017, 2020, Godeau et al., 2018, Rasbury et al., 2021]. Although technically challenging because of usual low U concentrations (<10 ppm) in calcite, the biggest benefit of LA-ICP-MS comes from the spatial resolution (less than ~100 µm) at which data can be obtained. Laser ablation spots on the order of 50–200 µm can be accurately placed to target single structural and compositional domains and combined to calculate a single date [Roberts and Holdsworth, 2022]. The current detection limit of U and Pb is low, ~0.1 ppm, and efforts are being made to still expand the limits of LA-ICP-MS detection [Kylander-Clark, 2020]. Generating ages and relating these ages to geological processes requires the combination of spatially resolved variations in composition (micron-scale elemental and isotopic mapping) and U–Pb isotopic concentrations. The integration of compositional image-based data with U–Pb data can be used to interpret and refine age data, either (1) by using independent imagery and analysis to target, refine, and interpret the U–Pb analyses that are based on static spot ablations, or (2) by using mapping tools to extract age data directly from the map itself, i.e., ages calculated from the pixel values [Drost et al., 2018, Hoareau et al., 2021a]. Ages are determined from isochrons in Tera-Wasserburg diagrams (e.g., by determining the lower intercepts using free regressions). For more details, the reader is referred to the papers by Guillong et al. [2020] and Roberts et al. [2020].

5.2. Limitations and way forward

A striking advantage of the U–Pb calcite dating technique applied to deformed rocks from FTBs and sedimentary basins is that it is not fraught with closure

temperature issues. Experimental data by Cherniak [1997] suggest that Pb diffusion in calcite is essentially slow enough to be non-existent below 300 °C, so recent LA-ICP-MS dating studies rely upon the idea that diffusion is unlikely in low-*T* calcite. However, at temperatures >400 °C, Pb diffusion is possible if encountered for long periods (>20 Myr) [Roberts et al., 2020]. Cruset et al. [2020] reported that U–Pb dating may fail in calcite cement from samples which have temperatures >110 °C and too high initial Pb/U contents, suggesting that temperature somehow could be a limiting parameter in the U–Pb dating method.

A key requirement for calcite geochronology is that detailed field (micro)structural and petrographic observations need to be carried out in order to unambiguously link the calcite growth history to the tectonic history. If some structures hosting synkinematic calcite mineralizations seem to be more consistently prone to return a reliable U–Pb age, such as crack-seals [Roberts and Holdsworth, 2022] or striated calcite steps along mesoscale faults [Beaudoin et al., 2020], it remains unclear, to date, what kind of parameters favors the success of U–Pb dating of a given tectonic structure. Only, one can say that some areas, or some lithotypes or stratigraphic layers are easier to date by U–Pb geochronology, regardless of the tectonic event the structure belongs to [e.g. Cruset et al., 2020, Mottram et al., 2020, Bilau et al., 2023]. At minimum one needs to ascertain the unambiguous coevality between calcite precipitation and deformation. In the case of veins, the timing of opening and cement precipitation may not be perfectly identical, and full cement precipitation may slightly postdate vein opening. The petrological outline of veins can help constrain the relative timing of opening and precipitation. For antitaxial veins, the precipitation rate equals or exceeds the opening rate, reflecting undoubtedly precipitation coeval with opening [Bons et al., 2012]. In contrast, blocky calcite indicates free precipitation of fluids in a void, due either to a fluid precipitating after joint development or to a fluid precipitating at slower rate than the rate of opening. The latter case can nevertheless reflect a coeval opening/precipitation timing if the precipitation is directly triggered by the opening of the veins. Within a vein set related to a given tectonic event, each vein may have developed at any time during the entire duration of the tectonic event. Thus, blocky calcite veins can reasonably be considered as reflect-

ing coeval vein opening/precipitation over the time span corresponding to the tectonic event that developed a given fracture set. However, one needs to ensure that the calcite filling did not precipitate during a subsequent deformation stage. A way to do so is to investigate the geochemical signature of the past fluids the calcite precipitated from, as the past fluid system usually evolved during deformation [Beaudoin et al., 2022]. In any case, one generally considers the oldest age gained from a vein population to provide a minimum bound for the onset age of the deformation stage the veins belong to.

The U–Pb dating of calcite-bearing mesostructures intrinsically suffers from several limitations. First, calcite does commonly incorporate more Pb than U, making it often difficult to date [Mottram et al., 2020]. Second, diagenetic and vein-fill calcite usually displays more variable and lower contents of U and higher contents of Pb than other types (e.g., speleothems), so U–Pb dating has a lower chance of success in this material [Roberts et al., 2020]. Third, there is still a lack of understanding of calcite recrystallization processes in the case of multiple stages of deformation and complex fluid history [Roberts et al., 2021]. The role of diagenesis on the incorporation of U and Pb in carbonate minerals remains debated [Roberts et al., 2020]. Thus, the diagenetic state of the calcite vein cement has to be systematically studied, along with its elementary content, in order to properly perform the analysis [Beaudoin et al., 2022]. U and Pb mobility assisted by fluid-flow in the fault zone is a common potential issue, so the age determined may not correspond to the true period of fault slip. Indeed, the age of the calcite mineralization can be younger than the fault activity because of a subsequent fluid flow. While Roberts et al. [2021] reported a reliable ~250 Ma age of slip along the Očkov thrust (Prague basin), another cross-cutting slicken-fiber yielded an apparent age at ~95 Ma which likely reflects a later Cretaceous fluid flow. This study illustrates that the careful geochemical, compositional and microstructural characterization of the calcite mineralization is a prerequisite to ensure that the calcite, and in particular, the dated isotopic system, has remained undisturbed by later structural, thermal or fluid-related activity [Roberts et al., 2021], hence for the safe tectonic interpretation of U–Pb dates. In the Bighorn basin (USA), Beaudoin et al. [2018] reported analytically reliable Mio–Pliocene ages for some veins

which geometry and relative chronology with respect to folding was consistent with the late Cretaceous–Paleogene Laramide contraction. This discrepancy was tentatively related to resetting linked to hot fluid circulation coeval with Yellowstone hotspot activity and Basin-and-Range extension. To check whether the U–Pb age legitimately represents that of calcite precipitation, a recent approach has coupled $\Delta^{47}\text{CO}_2$ paleothermometry to U–Pb geochronology to check the temperature of precipitation and a potential diagenetic alteration recorded by $\Delta^{47}\text{CO}_2$ temperature history reordering [Pagel et al., 2018, Hoareau et al., 2021b].

Should it be hampered by a primary lower U/higher Pb content or a possible complex history of fluid circulation, the reliable and meaningful dating of a given tectonic vein and mesoscale fault population is challenging and may require a large number of samples. For instance, the ages obtained from vein cements might not be straightforwardly interpreted as representative of the entire duration of the deformation event that developed the veins, so a certain number of data might be required to cover the entire timespan during which a deformation phase affected the rock [Beaudoin et al., 2018]. Overall, this questions the strategy of sampling a population of veins related to a given contractional stage, e.g. LPS, and the way to interpret the few, potentially scattered, discrete ages obtained from some individual veins out of this population when one aims at constraining the duration of the stage that expectedly largely exceeds the uncertainties on the U–Pb ages of individual veins. In other words, one can hardly reliably define the duration of a continuum of deformation from few discrete ages of some related mesostructures, except by dating a huge number of samples in order to reach a statistical representativity and to expect to be able to define the limits of the statistical distribution, hence the age of the onset and end of the fracturing event, which is practically not feasible.

The difficulty of interpreting ages from a necessarily limited number of analyses may also be encountered in fault zones. In repeatedly reactivated fault zones, which may consequently display multiple generations of cemented veins and cataclasites, a range of ages can be obtained from dating of a single fault. For instance, Corrêa et al. [2022] documented the Eocene reactivation as strike-slip fault of

a former Cretaceous normal fault in southern France. The eleven Eocene ages obtained from cements of veins and breccia from 3 samples from the fault zone range from 50 to 40 Ma (and even 55 to 35 Ma considering uncertainties). This scattering may be acceptable at first glance if one aims at placing the fault slip event within a long-lasting regional tectonic evolution. Alternatively, the range of ages is possibly informative of the duration of fault activity, here 10–20 Ma. The scattering of ages obtained from successive mesoscale fault or vein populations in a given area may however lead to overlapping ages despite a well constrained sequence of mesostructural development, so the interpretation of these ages may be challenging when one aims at dating folds in a recent and fast propagating FTB [Lacombe et al., 2021].

6. Discussion: how geochronology helps constrain the timing, sequence and rate of deformation in FTBs

K–Ar and U–Pb geochronology has been successfully applied in FTBs and broken forelands worldwide to date large-scale faults or microstructure alike from Paleozoic to Cenozoic [e.g., K–Ar: Lyons and Snellenburg, 1971, Vrolijk and van der Pluijm, 1999, van der Pluijm et al., 2001, Ylagan et al., 2002, Löbens et al., 2011, Duvall et al., 2011, Hnat and van der Pluijm, 2014, Paná and van der Pluijm, 2015, Curzi et al., 2020, Viola et al., 2018, Carboni et al., 2020, Fitz-Diaz et al., 2014, Wang et al., 2016, Hernández-Vergara et al., 2021, Haines and van der Pluijm, 2023; U–Pb: Rasbury and Cole, 2009, Ring and Gerdes, 2016, Hansman et al., 2018, Parrish et al., 2018, Beaudoin et al., 2018, 2020, Carminati et al., 2020, Smeraglia et al., 2021, Cruset et al., 2020, 2021, Looser et al., 2021, Hoareau et al., 2021b, Parizot et al., 2021, Lacombe et al., 2021, Pavlovskaja et al., 2022, Muñoz-López et al., 2022, Bilau et al., 2023]. The direct comparison of U–Pb carbonate and K–Ar illite fault dating methods [Mottram et al., 2020] shows the coincidence of periods of fracturing, calcite cementation and fluid flow with intervals of gouge-generating slip. The recognition of similar slip events from distinct fault-generated materials using different dating techniques supports the complementarity and the reliability of these methods for dating brittle fault slip. Keeping the limitations and pitfalls of each method in mind, K–Ar/Ar–Ar and U–Pb dating

of syn-kinematic illite and calcite, respectively, can be considered as providing reliable ages of tectonic (meso)structures.

While K–Ar illite dating requires suitable outcrop conditions and lithotypes to sample fault gouges, U–Pb calcite dating only needs very small calcite-bearing features that are nearly ubiquitous considering the abundance of calcite in sedimentary basins and FTBs. It thus becomes apparent that notwithstanding the cost of analyses, one can theoretically date as many calcite-bearing brittle mesostructures as needed to obtain a good coverage of ages for the different generations of mesostructures at several structural locations of a fold and for the entire stratigraphic section. In addition, one can expectedly obtain ages from poorly deformed domains devoid of any large-scale fault zones, including domains in between spatially separated large thrusts which activity can be dated using illite geochronology.

When dealing with the folding event, only the fold growth itself is associated with macroscopic deformation that could be reflected in depositional patterns, or linked with slip along a fault zone that can be dated using illite K–Ar geochronology. LPS and LSFT stages typically are not associated with significant amounts of deformation and are characterized by micro- and mesoscale deformation patterns only. As a result, the age of the onset and end of these stages, hence their duration, can only be assessed by means of dating related mineralized mesostructures with techniques such as U–Pb geochronology. In addition, the published fold dates obtained using K–Ar or Ar–Ar illite or muscovite geochronology mainly consist of single ages considering uncertainties and do not allow for estimating a duration of fold growth. In contrast, the dating of a population of syn-folding mesostructures may reveal a certain duration of fold growth despite uncertainties. The bracketing of fold growth age by the age of the youngest early-folding and of the oldest late-folding mesostructures, respectively, may provide an additional information, which altogether, grants access to the time period of fold growth even in the absence of growth strata.

The calcite U–Pb and illite K–Ar dating techniques are therefore complementary and the ages can be combined to constrain the timing of structural development in FTBs. It is important to note that from these dates, further information can be derived about the dynamics of FTBs [e.g. Cruset et al., 2021]. First,

the dates of different folds and thrusts in FTBs help constrain the sequence of structural development. Second, the dates can be used to derive the duration of fold growth but also of LPS and LSFT, which, in the case of LPS, is of prime interest since LPS is associated with substantial small-scale rock damage and corresponds to a key period for large-scale fluid flow and ore deposition in FTBs [Beaudoin et al., 2022]. Third, combined with estimates of shortening from section balancing across FTBs, these dates allow for calculating rates of shortening as well as rates of fold/thrust front propagation.

6.1. *Dating natural folding and thrusting events* (1): *sequence of deformation and orogenic wedge dynamics*

The absolute dating of folds and thrusts across FTBs reveals different sequences of structural development, and even the absence of any clear sequence in some places. Looser et al. [2021] reported U–Pb dates of calcite veins associated with a thrust branching off from the basal décollement in the distal Alpine Molasse Basin and slickenfibers from thrusts and strike-slip faults in the eastern Jura Mountains (Figure 4G,H). The ~15–4.5 Ma ages suggest earlier propagation of Alpine deformation into the distal foreland along the basal décollement than previously thought. Younger deformation ages (~11–4.5 Ma) support simultaneous tectonic activity along the Jura Mountains and the Subalpine Molasse thrust fronts. Smeraglia et al. [2021] reported thrust ages between ~12 and ~7 Ma in the central Jura Mountains which point to a thrust activity younging westwards and therefore to an in-sequence thrust propagation; the authors also documented the reactivation of pre-orogenic strike-slip faults as tear faults during Jura imbrication between ~10 and 5 Ma. Pană and van der Pluijm [2015] linked the tectonic history deduced from thrust dating in the Canadian Rockies to depositional patterns in the Western Canadian Sedimentary Basin, and proposed a forelandward sequence of thrusting from the late Jurassic until the Eocene (Figure 4A,B). Fitz-Diaz and van der Pluijm [2013] and Fitz-Diaz et al. [2014] have dated folds and shear zones within the Mexican FTB (Figure 4C,D). Ages indicate (1) shearing at ~84 Ma on the western edge of the Zimapán basin, then folding at ~82 Ma and localized shearing at ~77 Ma within the basin

and (2) folding at ~64 Ma and ~44 Ma on the western and eastern side of the Tampico–Misantla basin, respectively. These results are consistent with the age and distribution of syn-tectonic turbidites and indicate a forelandward propagation of the deformation. In contrast, Rahl et al. [2011] carried out integrated fault gouge dating with apatite fission-track thermochronometry in the southern Pyrenees to unravel the complex sequence of deformation that includes out-of-sequence thrusting. In the Western Alpine FTBs, U–Pb thrust ages of ~15 Ma to the east and 8 Ma to the west at the contact with the Miocene Molasse basin [Bilau et al., 2023] support an overall in-sequence thrust activation. However, in detail, younger ages in the innermost Bauges massif and in the Vercors massif indicate a later out-of-sequence activity. The concomitance between the eastern thrust activity and the period of rapid exhumation of the Belledonne External Crystalline Massif hints towards a possible effect of basement tectonics on the development of cover thrusts.

Beaudoin et al. [2018] reported U–Pb ages of calcite veins related to the Laramide contraction from the Rattlesnake Mountain anticline (RMA) in the west of the Bighorn basin and from the Sheep Mountain anticline (SMA) and the Bighorn Mountains (BM) in the east (Figure 4E,F). In SMA+BM, LPS lasted 72–50 Ma while fold growth occurred between 50 and 35 Ma. In RMA, LPS lasted 60–35 Ma and folding was active at least at 35–29 Ma. Even though the age of the onset of LPS is poorly constrained, these dates show that LPS and folding occurred earlier in the east, hence propagated in a westward sequence, thus violating the commonly accepted large-scale sequence of forelandward (eastward) younging deformation as deduced from syn-tectonic stratigraphy of sedimentary basins [e.g., Thacker and Karlstrom, 2019]. Interestingly, this opposite sequence of deformation is in line with low-*T* thermochronologic ages of rocks of the surrounding basement arches, with development of the earliest Laramide veins in the folded sedimentary cover being synchronous with the rapid phase of exhumation of their closest arches [Beaudoin et al., 2019]. This study reveals that the local sequence of thrusting/folding may change owing to strong structural inheritance. In contrast to thin-skinned orogenic wedges that often propagate/ accrete progressively outwards through time, thick-skinned systems may display a more irregular and erratic sequence

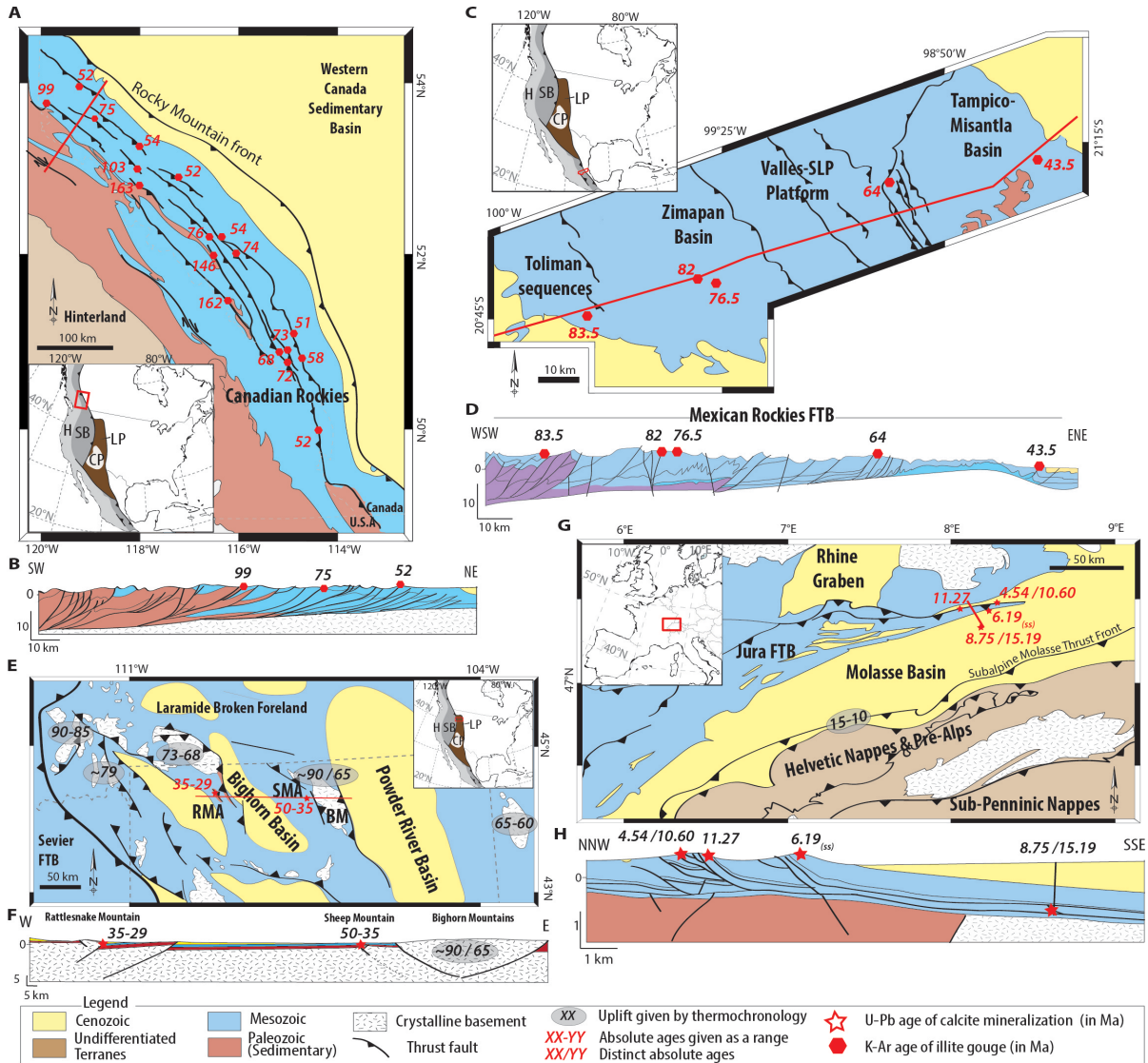


Figure 4. Simplified structural maps and cross sections in various FTBs, on which are reported the ages of fold and thrust activity obtained either by K–Ar/Ar–Ar illite or by U–Pb calcite geochronology. (A,B) Canadian FTB, after Pană and van der Pluijm [2015]; (C,D) Mexican FTB, after Fitz-Diaz et al. [2014]; (E,F) Laramide broken foreland, after Beaudoin et al. [2018, 2019] and Thacker and Karlstrom [2019]; (G,H) Jura FTB, after Looser et al. [2021]. H (Hinterland), SB (Sevier Belt), LP (Laramide Province), CP (Colorado Plateau). See text for details.

possibly linked to the heterogeneous and complex transmission of stress and accommodation of shortening through the crystalline basement with inherited weaknesses and anisotropies [Lacombe and Bellahsen, 2016]. Despite distinctive characteristics of basement involvement in shortening in the Laramide province and the Zagros, these results are consistent

with numerical experiments of basement-involved FTB development with or without inherited basement faults [Najafi et al., 2021]. Both the experiments show in-sequence folding advancing toward the foreland. In the model without inherited faults, the onset of folding is roughly continuous whereas the experiment with inherited basement faults displays a

more complex scenario with discontinuous onset of folding and local out-of-sequence propagation of deformation, probably related to the fact that inherited faults concentrate shortening in the basement.

Absolute ages of folds and thrusts in FTBs are informative on the past dynamics of the thrust wedge. The dating of thrusts reveals that (parts of) a FTB may have a complex internal dynamics, behaving either as a critically-stressed or a stable wedge during its growth. In the Jura, the seemingly continuous forelandward younging sequence of thrusting supports that the wedge moved stably above the weak Triassic evaporite decollement; however, the wedge dynamics was possibly more complex as revealed by the late reactivation of strike-slip faults related to the same contraction in the inner part of the wedge. Age dating also reveals that a FTB might not evolve as a single orogenic wedge that was at failure everywhere as the wedge grew. In some instances, rocks in the inner wedge deformed first, and after shortening and thickening, locked up and became the backstop that deformed rocks in the outer part, giving birth to a composite orogenic wedge made of spatially and temporally distinct successive belts and fronts. This results in some kind of pulse-like development of the orogenic wedge, the pulses corresponding to temporally discrete periods—lasting a few million years—characterized by rapid and temporally overlapping activity of spatially separated thrusts [Haines and van der Pluijm, 2023]. For instance, the ages obtained by van der Pluijm et al. [2006] from gouges of several thrusts in the Canadian Rockies reveal orogenic shortening in two distinct pulses (~72 and ~52 Ma) within a forelandward sequence, thrusting being episodic rather than gradual across the belt, which resulted in spatially and temporally distinct front ranges. These results show that large domains of FTBs underwent contraction at about the same time, which supports a critically-stressed, internally deforming, thrust wedge. Similarly, the K–Ar ages (50–46 Ma) of thrusts in the Sevier FTB of Wyoming [Solum and van der Pluijm, 2007] suggest that the thrusts deformed more or less synchronously, hence without clear sequence. The significance of these similar ages is demonstrated by the older age of the altered host rock along the frontal thrust, which indicates that the 50–46 Ma ages are not related to a regional fluid-flow event which would have homogenized isotopic signatures. Clay gouges of sev-

eral thrusts in the Appalachian foreland also exhibit identical ages within error [276–280 Ma, Hnat and van der Pluijm, 2014]. In the central Mexico FTB, the progressive but episodic (pulse-like) forelandward younging deformation and the absence of any out-of-sequence deformation ages also support that segments of the tectonic wedge may have remained relatively undeformed once incorporated into the wedge.

The pulse-type progression of deformation view challenges that of a continuous progression of deformation as in the Jura, leading authors to infer episodic deformation separated by periods of tectonic quiescence. Although the duration of the inferred quiescence periods is long and often cannot be accounted for by uncertainties associated with the age of the individual thrusts, one can wonder whether this signal is geologically significant or simply reflects the time needed for stress transmission and strain localization in a possibly hardening material, with possibly missed minor but continuous mesoscale deformation in between the major thrusts, that possibly would have been revealed by a more continuous sampling and U–Pb dating of distributed, mesoscale calcite-filled fractures. Alternatively, the quiescence may well be an artifact of the discontinuous sampling of fault gouges or even the difficulty for the technique to record all the stages of fault activity, possibly revealing a particular faulting increment only. Finally, one should not neglect the occurrence of aseismic deformation, hence strain being accommodated without discrete localization, thus without rupturing [e.g., Gratier and Gamond, 1990, Zuccari et al., 2022].

6.2. *Dating natural folding and thrusting events (2): duration of contractional stages at the fold scale and emplacement of thrust sheets*

Capturing the duration of a given continuous deformation stage is challenging and the safest way to do that is to bracket this stage by dating mesostructures that unambiguously preceded and postdated the deformation stage of interest as constrained by relative chronology. Indeed, it would be theoretically possible to capture the duration of a given deformation stage, e.g., LPS, by dating the syn-kinematic calcite

mineralization related to this stage. However, because the related mesostructures can develop quasi-instantaneously at any time of the LPS stage, it is practically impossible to ensure—and it is statistically unlikely as well—that the ages obtained from the necessarily limited number of samples cover the entire timespan during which the deformation stage affected the rock. In other words, it is impossible to ensure the oldest and youngest dated LPS-related veins correspond with certainty to the onset and end of LPS, respectively. The ages obtained might not be straightforwardly interpreted as representative of the entire duration of the deformation stage and one can at best consider that the oldest age obtained provides a minimum age for the onset of LPS, hence a minimum duration of LPS. U–Pb dating can also be applied to syn-folding mesostructures, and the difference between their oldest and youngest ages should be considered as the minimum duration of fold growth. To that respect, the discrete fracture time record of folding is much more discontinuous and fragmented than the growth strata record. Lastly, U–Pb dating can be used to constrain the time and duration of LSFT, but with the same limitation than for the other stages. The timing of fold growth can however be refined by considering the entire range of ages of the syn-folding mesostructures together with the youngest and oldest dates for LPS- and LSFT-related structures, respectively.

As emphasized by Lacombe et al. [2021], strata from which mesostructures are usually dated are mainly pre-folding strata and there have been few attempts at directly dating mesostructures developed within growth strata [Cruset et al., 2020]. The reason is that the often poorly indurated syn-folding formations are less prone to fracturing and calcite cementation at the time of deformation compared to pre-folding, well-indurated rocks. More generally, fracture studies in syn-tectonic strata are few, but a nice check of the ability of the U–Pb dating of syn-folding structures to capture the duration of fold growth would be to date syn-folding mesostructures in a fold for which the growth strata record is preserved and dated, and even to date fractures developed during growth strata deposition if any.

Beaudoin et al. [2018, 2020] and Lacombe et al. [2021] provided estimates of the duration of each stage of the folding event for various folds from different settings, using a combination of time mark-

ers like U–Pb ages from calcite-filling fracture sets and growth strata. For the Laramide SMA forced fold, LPS and fold growth lasted 20–25 Myr and ~15 Myr, respectively; the duration of the LSFT was bracketed between 35 Ma and ~17 Ma. For the Pico del Aguila detachment fold (southern Pyrenees), U–Pb ages combined with biostratigraphic dating of growth strata revealed that LPS, folding and LSFT lasted ~19 My (61–42 Ma), ~7 My (42–35 Ma) and ~17 My (35–18 Ma), respectively. In the San Vicino-Cingoli fault-bend fold pair (Apennines, Figure 5), U–Pb ages of veins related to LPS, folding and LSFT combined with existing time constraints [e.g., Calamita et al., 1994, Labeur et al., 2021] indicate that LPS lasted ~1 My (~6.5–5.5 Ma) for both anticlines, followed by fold growth lasting ~1.5–3 My (~5.5–~3.5 Ma). LSFT started ~5 Ma in the Camerino syncline [Beaudoin et al., 2020], ~4 Ma in San Vicino and ~3 Ma in Cingoli. The entire folding event lasted ~3–4 My [Lacombe et al., 2021; Figure 5]. Muñoz-López et al. [2022] reported U–Pb dating of calcite veins from the Boixols-Sant Corneli anticline (Pyrenees). Dates coeval with (~71–57 Ma) and postdating (55–27 Ma) growth strata deposition mark the emplacement of the Boixols thrust sheet and the growth of the Boixols-Sant Corneli anticline along its front, then the fold tightening during its late tectonic transport, respectively. These dates indicate that LPS + folding lasted ~14 My and that LSFT lasted ~28 My. U–Pb ages of fibers from beefs, veins and faults in the Neuquén Basin (Argentina) indicate that LPS lasted from 79 ± 10 to 61 ± 10 Ma, followed by two periods of syn-to post-folding contraction, 52 ± 3 to 42 ± 19 Ma and $\sim 14 \pm 3$ to 6 ± 1 Ma [Cruset et al., 2021]. Taking into account the rather large age uncertainties, the inferred durations are ~20 (–40?) My for LPS and 8–12 My to 10 (–30?) My for folding+LSFT.

U–Pb calcite geochronology therefore reveals that the growth of the studied folds lasted between 1.5 and 20 My, in line with estimates based either on growth strata [Holl and Anastasio, 1993, Anastasio et al., 2017, Najafi et al., 2021] or mechanical modeling [Yamato et al., 2011, Najafi et al., 2021]. This suggests that most folds would expectedly develop in less than 20 Ma regardless of the setting. The rapid growth of the San Vicino and Cingoli anticlines is consistent with the high rates of contraction and migration of deformation above a weak decollement in the Apennines, as observed in the

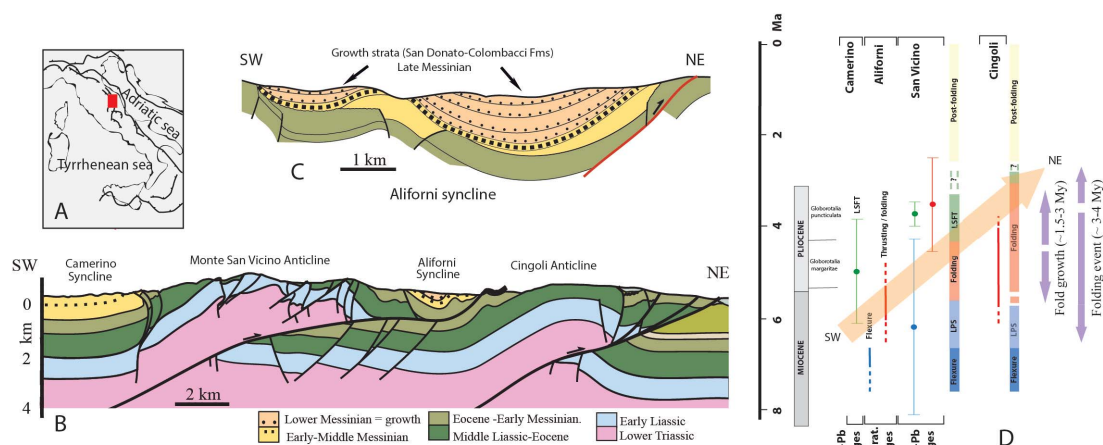


Figure 5. Location (A) and cross-sections (B) of the San Vicino and Cingoli anticlines and the Aliforni syncline [after Mazzoli et al., 2002], with compilation of age constraints on the timing and duration of fold growth and folding event, with inferred eastwards younging folding sequence (light orange big arrow).

Zagros [Najafi et al., 2021]. In contrast, fold growth lasted longer in the case of forced folding above a high angle basement thrust (SMA) compared to fault-bend folding (San Vicino and Cingoli) along a flat-ramp decollement and detachment folding (Pico del Aguila) above a weak decollement. These results are consistent with the numerical experiments of basement-involved orogenic wedge development [Najafi et al., 2021], in which the propagation of the onset of folding is continuous and anticlines grow for a limited time period of a few million years in the model without inherited faults, whereas the experiment with reactivated inherited basement faults reveals a longer duration of anticline growth.

Concerning LPS, its longer duration in SMA compared to Pico del Aguila, San Vicino, Cingoli and Boixols-Sant Cornelli reflects to some degree the longer duration of the stress/strain accumulation required to initiate forced folding of the undetached sedimentary cover above an inverted high angle basement normal fault than to initiate cover folding above a weak decollement. The longer LPS at Pico del Aguila with respect to San Vicino, Cingoli and Boixols-Sant Cornelli may be related to its development oblique to the regional compression in contrast to the other folds which instead developed perpendicular to it [Lacombe et al., 2021].

Finally, LSFT appears to last longer when folding is anchored to a high angle basement thrust (SMA), but also when the fold is located at the front of the

orogenic wedge, i.e., when the later propagation of deformation is limited or slow, or when folding occurs in a complex sequence (Pico del Aguila, SMA, Boixols-Sant Cornelli). The relatively short LSFT in San Vicino and Cingoli folds is, like their rapid growth, in line with the high rate of migration of deformation [Lacombe et al., 2021]. These results suggest that the duration of each deformation stage of the folding event depends on the structural style and/or the regional sequence of deformation.

Information about the duration of thrust sheet emplacement and thrust activity from U-Pb geochronology is scarce. In the SE Pyrenees, the Late Cretaceous to Oligocene piggy-back thrust sequence consists of the stacking, from top-and-older to bottom-and-younger, of the Bóixols-Upper Pedraforca, the Lower Pedraforca and the Cadí thrust sheets, and the Ebro foreland basin. The U-Pb ages of veins collected within the thrust sheets or in the damage zones of the sole thrusts [Cruset et al., 2020] fit with the timing of deformation as constrained by growth strata, but also provide further information on the duration of emplacement of thrust units. In this sense, dates from the Bóixols-Upper Pedraforca unit reflect its emplacement (~71–55.3 Ma) as well as its subsequent deformation (~49–26 Ma) when the Lower Pedraforca unit, then the Cadí unit, was emplaced in sequence. Similarly the Lower Pedraforca unit was deformed during its emplacement (48–41 Ma) but also during the emplacement of the Cadí unit. The

39–26 Ma dates from the Cadí unit are coeval with growth strata within the foreland. Durations of thrust sheet emplacement are in the ranges 15.3–18.8 My, 7.3–11.6 My and 12.9–14.3 My for the Bóixols–Upper Pedraforca, Lower Pedraforca and Cadí units, respectively. This 8–19 My range of values compares well to the 1.5–20 My range of duration of folding, which may indicate a similar order of magnitude of duration for folding and thrust sheet emplacement in FTBs. Interestingly, even though its kinematics is still a matter of debate (thrust versus low-angle normal fault), the recent K–Ar illite dating of the fault rocks of the exhumed Zuccale fault (Elba, Italy) also reveals a similar ~20 Myr long kinematic history during the Tertiary evolution of the Northern Apennines.

Attempts at estimating the duration of the thrust activity itself from direct dating of structures within the fault zone using U–Pb face the large variability in the ages of syn-kinematic mineralizations in a given part of the fault zone, i.e., following the vertical extension of the fault, where a number of discrete slip events can be recorded [e.g. Corrêa et al., 2022]. This kind of results gives hope that geochronology will help better constrain the entire timespan during which the fault was active, even though the cumulated duration of the discontinuous (co-seismic?) slip increments may be much shorter than this timespan. Because (thrust) faults are also commonly segmented, the absolute age of activity of a fault (i.e. in map-view) also show some variability (Figures 4A,B and 6). The precise appraisal of the duration of thrust activity remains a challenging task to date.

6.3. *Dating natural folding and thrusting events (3): shortening rate and thrust/fold front propagation rate*

Absolute ages of folding and thrusting can be combined with kinematic constraints and shortening estimates from the sequential restoration of local or regional balanced cross sections to constrain individual fold growth rates and regional shortening rates. Deformation front propagation rates can be constrained as well if the successive frontal thrusts can be both dated and restored through time. Very few shortening rate estimates have been obtained to date from combined sequential restoration of balanced cross sections and U–Pb dating of deformation along these sections. The more recent campaigns

of fold and thrust absolute dating in FTBs have focused on the timing and sequence of structural development and were unfortunately very rarely conducted in parallel with sequential restoration of the investigated cross section. The U–Pb dates obtained by Cruset et al. [2021] in the SE Pyrenees nappe stack combined with previous shortening estimates by section balancing and restoration indicate maximum shortening rates of 0.6–0.7 mm/yr for the Bóixols–Upper Pedraforca, 3.1–4.9 mm/yr for the Lower Pedraforca and 1.1–1.3 mm/yr for the Cadí thrust units. These estimates well compare to earlier estimates based on stratigraphic constraints, e.g., the initial emplacement of the Pedraforca thrust sheet (58–54 Ma) and development of the Pedraforca breakback thrusts (47.5–40 Ma) at a mean shortening rate of 2.4 mm/yr [Burbank et al., 1992]. U–Pb ages of successive thrusts across the Vercors recently acquired by Bilau et al. [2023] allow calculation of a local shortening rate (Figure 6). Using serial restored cross sections independently constructed by Philippe [1995] across the Vercors, one of those incidentally being limited by two in-sequence thrusts of which the activity was successfully dated, we calculated a shortening rate of ~2.2 mm/yr (from 1.4 mm/yr to 5.4 mm/yr when considering uncertainties on U–Pb ages). The two estimated mean shortening rates above (0.6–5 mm/yr) are roughly of the same order of magnitude than the short-term shortening rates either across individual folds [e.g., Simoes et al., 2007] or determined at a more regional scale using distributed faults and folds [Thompson et al., 2002], keeping in mind that local short-term rates may only reflect part of the total rates as derived from GPS and may not be representative of longer-term average shortening rates [Fu et al., 2017; see also Section 2.3].

We wish to draw the attention onto the paucity of available shortening rates so far. While this is partially explained by the relatively recent democratization of geochronology in this context, an effort still needs to be done by the community. Obtaining the shortening rate *a posteriori* by combining studies is arguable and quite complicated, as ages along a fault in map view can vary and the restoration of a cross section is valid only locally. Then, we invite future researchers to go beyond simple dating of folds and thrusts and to provide restored cross sections when possible

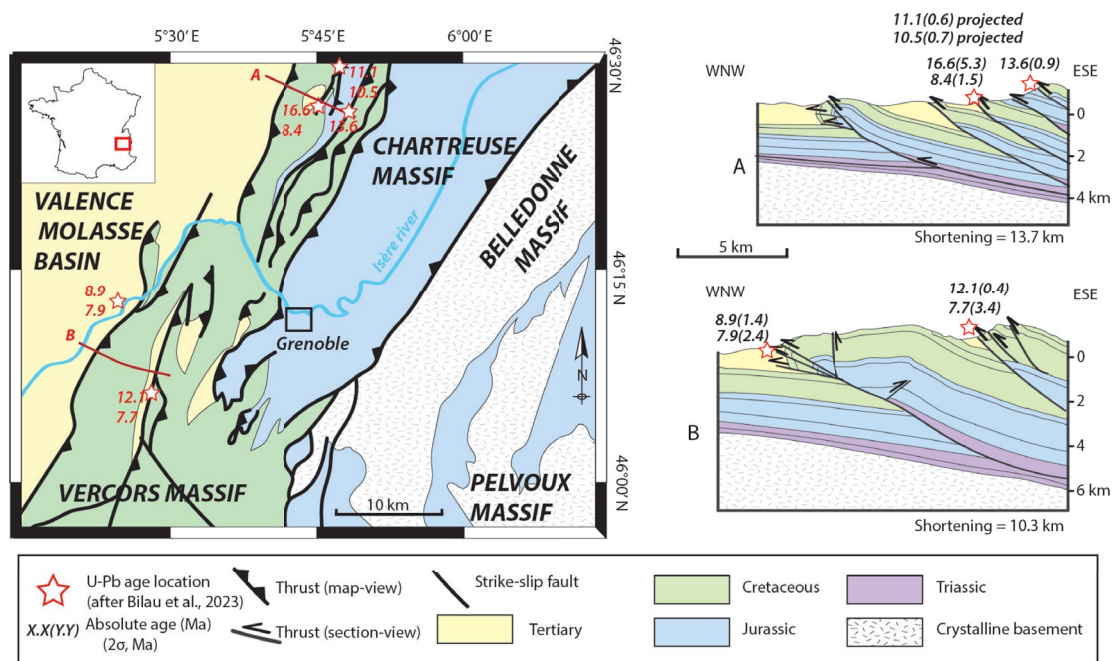


Figure 6. Structural map of the southwestern Subalpine FTBs with balanced cross sections across the southern Chartreuse (A) and the northern Vercors (B) [modified from Philippe, 1995] on which U-Pb thrust ages [Bilau et al., 2023] are reported. Section B has been used to estimate a local shortening rate.

to provide rates of deformation processes which are key to understanding how the (upper) crust deforms.

7. Conclusion

This review emphasizes how geochronology applied to absolute dating of folds, faults and fractures in fold-and-thrust belts complement classical approaches mainly based on the sedimentary record and provides new key insights into the timing, sequence, duration and rate of deformation. Increasing the regional absolute age datasets helps unravel the main faulting and folding episodes, thus bridging the gap that the study of only a single structure could be leading to. Clearly the more we date, the clearer the pattern of regional thrusting and folding. The extensive combination of absolute dates of folding and thrusting with independent studies using classical time markers makes it increasingly easier to depict a full picture of the main events forming and deforming a FTB.

Absolute dates for folding and thrusting not only support and refine a regional tectonic history, but

also enable us to quantify the duration and rate of shortening accommodated at the mesoscale and the macroscale, as well as the rate of propagation of deformation. This information, available by multiplying the data collection in mesoscale and large-scale thrusts and folds, should allow to more precisely address the rheological behavior of the upper crust and to either feed or validate quantitatively the predictions of analogue and numerical models of crustal deformation. Efforts should be made to still improve the resolution of the techniques and to ensure a sound tectonic interpretation of the dates obtained by conducting prior crystallographic, petrological, geochemical and microstructural characterization of the dated material. Despite their limitations, the absolute dating techniques are undoubtedly quantitative tools of primary importance that need to be combined with the often more continuous sedimentary record for a better description and understanding of the deformation processes at work in the shallow crust.

Conflicts of interest

Authors have no conflict of interest to declare.

Acknowledgements

The authors would like to thank Sylvie Leroy for soliciting a contribution from us to the Special Issue of the *Comptes Rendus Geoscience* dedicated to Jean Aubouin, as well as Giulio Viola and an anonymous reviewer for their constructive comments that helped improve the manuscript.

References

- Aldega, L., Viola, G., Casas-Sainz, A., Marcén, M., Román-Berdiel, T., and van der Lelij, R. (2019). Unraveling multiple thermotectonic events accommodated by crustal-scale faults in Northern Iberia, Spain: insights from K–Ar dating of clay gouges. *Tectonics*, 38(10), 3629–3651.
- Altaner, S. P. and Ylagan, R. F. (1997). Comparison of structural models of mixed-layer illite/smectite and reaction mechanisms of smectite illitization. *Clays Clay Miner.*, 45, 517–533.
- Anastasio, D., Kodama, K., and Parés, J. (2017). Episodic deformation rates recovered from growth strata, Pyrenees, search and discovery, AAPG datapages/search and discovery article #90291. In *AAPG Annual Convention and Exhibition, Houston, Texas, 2–5 April 2017*.
- Andersen, M. B., Stirling, C. H., Potter, E.-K., Halliday, A. N., Blake, S. G., McCulloch, M. T., Ayling, B. F., and O'Leary, M. (2008). High-precision U-series measurements of more than 500,000 year old fossil corals. *Earth Planet. Sci. Lett.*, 265(1–2), 229–245.
- Arne, D., Worley, B., Wilson, C., Chen, S., Foster, D., Luo, Z., Liu, S., and Dirks, P. (1997). Differential exhumation in response to episodic thrusting along the eastern margin of the Tibetan Plateau. *Tectonophysics*, 280, 239–256.
- Ault, A. K., Reiners, P. W., Evans, J. P., and Thomson, S. N. (2015). Linking hematite (U–Th)/He dating with the microtextural record of seismicity in the Wasatch fault damage zone, Utah, USA. *Geology*, 43(9), 771–774.
- Bar, E., Nuriel, P., Kylander-Clark, A., and Weinberger, R. (2021). Towards in situ U–Pb dating of dolomite. *Geochronology*, 3, 337–349.
- Beaudoin, N., Labeur, A., Lacombe, O., Koehn, D., Billi, A., Hoareau, G., Boyce, A., John, C. M., Marchegiano, M., Roberts, N. M., Millar, I. L., Claverie, F., Pecheyran, C., and Callot, J. P. (2020). Regional-scale paleofluid system across the Tuscan Nappe–Umbria Marche Apennine Ridge (northern Apennines) as revealed by mesostructural and isotopic analyses of stylolite-vein networks. *Solid Earth*, 11, 1617–1641.
- Beaudoin, N., Lacombe, O., Hoareau, G., and Callot, J. P. (2022). How the geochemistry of syn-kinematic calcite cements depicts past fluid flow and assists structural interpretations: a review of concepts and applications in orogenic forelands. *Geol. Mag.*, 159(11–12), 2157–2190.
- Beaudoin, N., Lacombe, O., Roberts, N. M. W., and Koehn, D. (2018). U–Pb dating of calcite veins reveals complex stress evolution and thrust sequence in the Bighorn Basin, Wyoming, USA. *Geology*, 46, 1015–1018.
- Beaudoin, N., Lacombe, O., Roberts, N. M. W., and Koehn, D. (2019). U–Pb dating of calcite veins reveals complex stress evolution and thrust sequence in the Bighorn Basin, Wyoming, USA: Reply. *Geology*, 47(9), article no. e481.
- Bilau, A., Bienvegnant, D., Rolland, Y., Schwartz, S., Godeau, N., Guihou, A., Deschamps, P., Mangelot, X., Brigaud, B., Boschetti, L., and Dumont, T. (2023). The tertiary structuration of the western subalpine foreland deciphered by calcite-filled faults and veins. *Earth-Sci. Rev.*, 236, article no. 104270.
- Boles, A., Schleicher, A. M., Solum, J., and van der Pluijm, B. (2018). Quantitative X-ray powder diffraction and the illite polytype analysis method for direct fault rock dating: a comparison of analytical techniques. *Clays Clay Miner.*, 66(3), 220–232.
- Bons, P. D., Elburg, M. A., and Gomez-Rivas, E. (2012). A review of the formation of tectonic veins and their microstructures. *J. Struct. Geol.*, 43, 33–62.
- Burbank, D. W., Puigdefàbregas, C. A. I., and Munoz, J. A. (1992). The chronology of the Eocene tectonic and stratigraphic development of the eastern Pyrenean foreland basin, northeast Spain. *Geol. Soc. Am. Bull.*, 104(9), 1101–1120.
- Butler, R. W. H. and Lickorish, W. H. (1997). Using high-resolution stratigraphy to date fold and thrust activity: examples from the Neogene of south-central Sicily. *J. Geol. Soc.*, 154, 633–643.

- Calamita, F., Cello, G., Deiana, G., and Paltrinieri, W. (1994). Structural styles, chronology rates of deformation, and time–space relationships in the Umbria-Marche thrust system (central Apennines, Italy). *Tectonics*, 13, 873–881.
- Carboni, F., Viola, G., Aldega, L., van der Lelij, R., Brozzetti, F., and Barchi, M. R. (2020). K–Ar fault gouge dating of Neogene thrusting: the case of the siliciclastic deposits of the Trasimeno Tectonic Wedge (Northern Apennines, Italy). *Ital. J. Geosci.*, 139(2), 300–308.
- Carminati, E., Aldega, L., Smeraglia, L., Scharf, A., Mattern, F., Albert, R., and Gerdes, A. (2020). Tectonic evolution of the northern Oman mountains, part of the strait of Hormuz syntaxis: new structural and paleothermal analyses and U–Pb dating of synkinematic calcite. *Tectonics*, 39(4), article no. e2019TC005936.
- Carrigan, J. H., Anastasio, D. J., Kodama, K. P., and Parés, J. M. (2016). Fault-related fold kinematics recorded by terrestrial growth strata, Sant Llorenç de Morunys, Pyrenees Mountains, NE Spain. *J. Struct. Geol.*, 91, 161–176.
- Cerling, T. E. and Craig, H. (1994). Geomorphology and in-situ cosmogenic isotopes. *Annu. Rev. Earth Planet. Sci.*, 22, 273–317.
- Chen, H., Yang, S., Picotti, V., Cheng, X., Lin, X., and Li, K. (2022). The late Cenozoic expansion of the northeastern Pamir: insights from the stratigraphic architecture of the Wupoer Piggyback basin. *J. Asian Earth Sci.*, 232, article no. 105012.
- Cherniak, D. J. (1997). An experimental study of strontium and lead diffusion in calcite, and implications for carbonate diagenesis and metamorphism. *Geochim. Cosmochim. Acta*, 61, 4173–4179.
- Clauer, N. (2013). The K–Ar and $^{40}\text{Ar}/^{39}\text{Ar}$ methods revisited for dating fine-grained K-bearing clay minerals. *Chem. Geol.*, 354, 163–185.
- Clauer, N., Srodon, J., Francu, J., and Sucha, V. (1997). K–Ar dating of illite fundamental particles separated from illite-smectite. *Clay Miner.*, 32, 181–196.
- Clauer, N., Zwingmann, H., Liewig, N., and Wendling, R. (2012). Comparative $^{40}\text{Ar}/^{39}\text{Ar}$ and K–Ar dating of illite-type clay minerals: a tentative explanation for age identities and differences. *Earth-Sci. Rev.*, 115, 76–96.
- Corrêa, R. S., Ukar, E., Laubach, S. E., Aubert, I., Lamarche, J., Wang, Q., Stockli, D. F., Stockli, L. D., and Larson, T. E. (2022). Episodic reactivation of carbonate fault zones with implications for permeability—an example from Provence, south-east France. *Mar. Pet. Geol.*, 145, article no. 105905.
- Cox, N. L. (2009). *Variable uplift from quaternary folding along the northern coast of east Timor, based on U-series age determinations of coral terraces*. PhD thesis, Brigham Young University. Unpublished.
- Cruset, D., Vergés, J., Albert, R., Gerdes, A., Benedicto, A., Cantarero, I., and Travé, A. (2020). Quantifying deformation processes in the SE Pyrenees using U–Pb dating of fracture-filling calcites. *J. Geol. Soc.*, 177(6), 1186–1196.
- Cruset, D., Vergés, J., Rodrigues, N., Belenguer, J., Pascual-Cebrian, E., Almar, Y., Perez-Caceres, I., Macchiavelli, C., Trave, A., Beranoaguirre, A., Albert, R., Gerdes, A., and Messenger, G. (2021). U–Pb dating of carbonate veins constraining timing of beef growth and oil generation within Vaca Muerta formation and compression history in the Neuquén basin along the Andean fold and thrust belt. *Mar. Pet. Geol.*, 132, article no. 105204.
- Curzi, M., Aldega, L., Bernasconi, S. M., Berra, F., Billi, A., Boschi, C., Franchini, S., Van der Lelij, R., Viola, G., and Carminati, E. (2020). Architecture and evolution of an extensionally-inverted thrust (Mt. Tancia Thrust, Central Apennines): geological, structural, geochemical, and K–Ar geochronological constraints. *J. Struct. Geol.*, 136, article no. 104059.
- DeCelles, P. G., Carrapa, B., and Gehrels, G. E. (2007). Detrital zircon U–Pb ages provide provenance and chronostratigraphic information from Eocene synorogenic deposits in northwestern Argentina. *Geology*, 35(4), 323–326.
- Delcaillau, B. (2001). Geomorphic response to growing fault-related folds: example from the foothills of central Taiwan. *Geodinam. Acta*, 14(5), 265–287.
- Drost, K., Chew, D., Petrus, J. A., Scholze, F., Woodhead, J. D., Schneider, J. W., and Harper, D. A. (2018). An image mapping approach to U–Pb LA-ICP-MS carbonate dating and applications to direct dating of carbonate sedimentation. *G-cubed*, 19, 4631–4648.
- Duvall, A. R., Clark, M. K., van der Pluijm, B. A., and Li, C. (2011). Direct dating of Eocene reverse faulting in northeastern Tibet using Ar-dating of fault clays and low-temperature thermochronometry. *Earth Planet. Sci. Lett.*, 304(3–4), 520–526.

- Eggins, S. M., Grün, R., McCulloch, M. T., Pike, A. W., Chappell, J., Kinsley, L., Mortimer, G., Shelley, M., Murray-Wallace, C. V., Spotl, C., and Taylor, L. (2005). In situ U-series dating by laser-ablation multi-collector ICPMS: new prospects for Quaternary geochronology. *Quat. Sci. Rev.*, 24, 2523–2538.
- Elisha, B., Nuriel, P., Kylander-Clark, A., and Weinberger, R. (2021). Towards in situ U–Pb dating of dolomite. *Geochronology*, 3, 337–349.
- Fitz-Diaz, E., Hudleston, P., Tolson, G., and van der Pluijm, B. (2014). Progressive, episodic deformation in the Mexican Fold–Thrust Belt (Central Mexico): evidence from isotopic dating of folds and faults. *Int. Geol. Rev.*, 56(6), 734–755.
- Fitz-Diaz, E. and van der Pluijm, B. (2013). Fold dating: a new Ar/Ar illite dating application to constrain the age of deformation in shallow crustal rocks. *J. Struct. Geol.*, 54, 174–179.
- Fredin, O., Viola, G., Zwingmann, H., Sørli, R., Brönnner, M., Lie, J. E., Grandal, E. M., Müller, A., Margreth, A., Vogt, C., and Knies, J. (2017). The inheritance of a Mesozoic landscape in western Scandinavia. *Nat. Commun.*, 8(1), 1–11.
- Fu, X., Li, S. H., Li, B., and Fu, B. (2017). A fluvial terrace record of late quaternary folding rate of the Anjihai anticline in the northern piedmont of Tian Shan, China. *Geomorphology*, 278, 91–104.
- Godeau, N., Deschamps, P., Guihou, A., Leonide, P., Tendil, A., Gerdes, A., Hamelin, B., and Girard, J. (2018). U–Pb dating of calcite cement and diagenetic history in microporous carbonate reservoirs: case of the Urgonian Limestone, France. *Geology*, 46(3), 247–250.
- Gosse, J. C. and Phillips, F. M. (2001). Terrestrial in situ cosmogenic nuclides: theory and application. *Quat. Sci. Rev.*, 20(14), 1475–1560.
- Grathoff, G. H. and Moore, D. M. (1996). Illite polytype quantification using WILDFIRE-calculated patterns. *Clays Clay Miner.*, 44, 835–842.
- Gratier, J. P. and Gamond, J. F. (1990). Transition between seismic and aseismic deformation in the upper crust. *Geol. Soc., Lond., Spec. Publ.*, 54(1), 461–473.
- Guillong, M., Wotzlaw, J. F., Looser, N., and Laurent, O. (2020). Evaluating the reliability of U–Pb laser ablation inductively coupled plasma mass spectrometry (LA-ICP-MS) carbonate geochronology: matrix issues and a potential calcite validation reference material. *Geochronology*, 2, 155–167.
- Haghipour, N., Burg, J. P., Kober, F., Zeilinger, G., Ivy-Ochs, S., Kubik, P. W., and Faridi, M. (2012). Rate of crustal shortening and non-Coulomb behaviour of an active accretionary wedge: the folded fluvial terraces in Makran (SE, Iran). *Earth Planet. Sci. Lett.*, 355, 187–198.
- Haines, S. H. and van der Pluijm, B. A. (2008). Clay quantification and Ar–Ar dating of synthetic and natural gouge: application to the Miocene Sierra Mazatán detachment fault, Sonora, Mexico. *J. Struct. Geol.*, 30(4), 525–538.
- Haines, S. H. and van der Pluijm, B. A. (2023). Fault gouge dating in the Spanish Pyrenees: fault ages, thrust propagation sequence, wall-rock provenance, and thermal constraints. *Tectonics*, 42, article no. e2022TC007251.
- Hansman, R. J., Albert, R., Gerdes, A., and Ring, U. (2018). Absolute ages of multiple generations of brittle structures by U–Pb dating of calcite. *Geology*, 46, 207–210.
- Heermance, R. V., Chen, J., Burbank, D. W., and Miao, J. (2008). Temporal constraints and pulsed Late Cenozoic deformation during the structural disruption of the active Kashi foreland, northwest China. *Tectonics*, 27(6), article no. TC6012.
- Hernández-Vergara, R., Fitz-Díaz, E., Brocard, G., and Morán-Zenteno, D. J. (2021). Illite ^{40}Ar – ^{39}Ar dating of Eocene deformation in the Chiapas Fold and Thrust Belt, southern Mexico. *Geol. Soc., Lond., Spec. Publ.*, 504(1), 315–341.
- Hinnov, L. A. (2013). Cyclostratigraphy and its revolutionizing applications in the earth and planetary sciences. *Geol. Soc. Am. Bull.*, 125(11–12), 1703–1734.
- Hnat, J. S. and van der Pluijm, B. A. (2014). Fault gouge dating in the southern Appalachians, USA. *Geol. Soc. Am. Bull.*, 126(5–6), 639–651.
- Hoareau, G., Claverie, F., Pecheyran, C., Paroissin, C., Grignard, P.-A., Motte, G., Chailan, O., and Girard, J.-P. (2021a). Direct U–Pb dating of carbonates from micron-scale femtosecond laser ablation inductively coupled plasma mass spectrometry images using robust regression. *Geochronology*, 3(1), 67–87.
- Hoareau, G., Crognier, N., Lacroix, B., Aubourg, C., Roberts, N. W., Niemi, N., Branellec, M., Beaudoin, N. E., and Suárez Ruiz, I. (2021b). Combination of $\Delta 47$ and U–Pb dating in tectonic calcite veins unravel the last pulses related to the Pyrenean Short-

- ening (Spain). *Earth Planet. Sci. Lett.*, 553, article no. 116636.
- Holl, J. E. and Anastasio, D. J. (1993). Paleomagnetically derived folding rates, southern Pyrenees, Spain. *Geology*, 21, 271–274.
- Homke, S., Vergés, J., Garcés, M., Emami, H., and Karpuz, R. (2004). Magnetostratigraphy of Miocene-Pliocene Zagros foreland deposits in the front of the Push-e Kush Arc (Lurestan Province, Iran). *Earth Planet. Sci. Lett.*, 225, 397–410.
- Hu, X., Pan, B., Fan, Y., Wang, J., Hu, Z., Cao, B., Li, Q., and Geng, H. (2017). Folded fluvial terraces in a young, actively deforming intramontane basin between the Yumu Shan and the Qilian Shan mountains, NE Tibet. *Lithosphere*, 9(4), 545–560.
- Hunziker, J. C., Frey, M., Clauer, N., Dallmeyer, R. D., Friedrichsen, H., Flehmig, W., Hochstrasser, K., Roggwiler, P., and Schwander, H. (1986). The evolution of illite to muscovite: mineralogical and isotopic data from the Glarus Alps, Switzerland. *Contrib. Mineral. Petrol.*, 92(2), 157–180.
- Khadivi, S., Mouthereau, F., Larrasoana, J.-C., Vergés, J., Lacombe, O., Khademi, E., Beamud, E., Melinte-Dobrinescu, M., and Suc, J.-P. (2010). Magnetostratigraphy of synorogenic Miocene foreland sediments in the Fars arc of the Zagros Folded Belt (SW Iran). *Basin Res.*, 22, 918–932.
- Kylander-Clark, A. R. C. (2020). Expanding the limits of laser-ablation U–Pb calcite geochronology. *Geochronology*, 2(2), 343–354.
- Labeur, A., Beaudoin, N. E., Lacombe, O., Emmanuel, L., Petracchini, L., Daëron, M., Klimowicz, S., and Callot, J.-P. (2021). Burial-deformation history of folded rocks unraveled by fracture analysis, stylolite paleopiezometry and vein cement geochemistry: a case study in the Cingoli Anticline (Umbria-Marche, Northern Apennines). *Geosciences*, 11, article no. 135.
- Lacombe, O., Beaudoin, N., Hoareau, G., Labeur, A., Pecheyran, C., and Callot, J. P. (2021). Dating folding beyond folding, from layer-parallel shortening to fold tightening, using mesostructures: Lessons from the Apennines, Pyrenees and Rocky Mountains. *Solid Earth*, 12(10), 2145–2157.
- Lacombe, O. and Bellahsen, N. (2016). Thick-skinned tectonics and basement-involved fold–thrust belts: insights from selected Cenozoic orogens. *Geol. Mag.*, 153, 763–810.
- Lanson, B., Beaufort, D., Berger, G., Bauer, A., Casagabere, A., and Meunier, A. (2002). Authigenic kaolin and illitic minerals during burial diagenesis of sandstones: a review. *Clay Miner.*, 37(1), 1–22.
- Lashgari, A., Heyhat, M. R., Vergés, J., Beamud, E., Najafi, M., Khatib, M., and Karimnejad, H. R. (2020). Age of synorogenic deposits and timing of folding in Dezful Embayment, SW Zagros Fold Belt. *Mar. Pet. Geol.*, 113, article no. 104148.
- Lavé, J. and Avouac, J. P. (2000). Active folding of fluvial terraces across the Siwaliks Hills, Himalayas of central Nepal. *J. Geophys. Res. Solid Earth*, 105(B3), 5735–5770.
- Lickorish, W. H. and Ford, M. (1998). Sequential restoration of the external Alpine Digne thrust system, SE France, constrained by kinematic data and synorogenic sediments. *Geol. Soc., Lond., Spec. Publ.*, 134(1), 189–211.
- Lin, Y., Jochum, K. P., Scholz, D., Hoffmann, D. L., Stoll, B., Weis, U., and Meinrat, O. A. (2017). In-situ high spatial resolution LA-MC-ICPMS $^{230}\text{Th}/\text{U}$ dating enables detection of small-scale age inversions in speleothems. *Solid Earth Sci.*, 2(1), 1–9.
- Livio, F., Sileo, G., and Michetti, A. M. (2007). Pleistocene compressive tectonics in Central Southern Alps (Italy): rates of folding determined from growth strata. In *Geophysical Research Abstracts*, volume 9, page 02740. European Geosciences Union.
- Löbens, S., Bense, F. A., Wemmer, K., Dunkl, I., Costa, C. H., Layer, P., and Siegesmund, S. (2011). Exhumation and uplift of the Sierras Pampeanas: preliminary implications from K–Ar fault gouge dating and low-T thermochronology in the Sierra de Comechingones (Argentina). *Int. J. Earth Sci.*, 100(2), 671–694.
- Lock, J. and Willett, S. (2008). Low-temperature thermochronometric ages in fold-and-thrust belts. *Tectonophysics*, 456(3–4), 147–162.
- Looser, N., Madritsch, H., Guillong, M., Laurent, O., Wohlwend, S., and Bernasconi, S. M. (2021). Absolute age and temperature constraints on deformation along the basal décollement of the Jura fold- and-thrust belt from carbonate U–Pb dating and clumped isotopes. *Tectonics*, 40(3), article no. e2020TC006439.
- Lyons, J. B. and Snellenburg, J. (1971). Dating faults. *Geol. Soc. Am. Bull.*, 82(6), 1749–1752.
- Mancktelow, N., Zwingmann, H., Campani, M., Füh-

- genschuh, B., and Mulch, A. (2015). Timing and conditions of brittle faulting on the silltal-brenner fault zone, eastern alps (Austria). *Swiss J. Geosci.*, 108, 305–326.
- Masaferro, J. L., Bulnes, M., Poblet, J., and Eberli, G. P. (2002). Episodic folding inferred from syntectonic carbonate sedimentation: the Santaren anticline, Bahamas foreland. *Sedim. Geol.*, 146, 11–24.
- Mazzoli, S., Deiana, G., Galdenzi, S., and Cello, G. (2002). Miocene fault-controlled sedimentation and thrust propagation in the previously faulted external zones of the Umbria-Marche Apennines, Italy. *EGU Stephan Mueller Spec. Publ. Ser.*, 1, 195–209.
- McArthur, J. M., Howarth, R. J., and Shields, G. A. (2012). In *Strontium Isotope Stratigraphy. The Geologic Time Scale 2012*, pages 127–144. Elsevier, Boston. Chapter 7.
- McClay, K. (1992). Glossary of thrust tectonics terms. In McClay, K., editor, *Thrust Tectonics*, pages 419–433. Chapman & Hall, London.
- McQuarrie, N., Horton, B. K., Zandt, G., Beck, S., and DeCelles, P. G. (2005). Lithospheric evolution of the Andean fold-thrust belt, Bolivia, and the origin of the central Andean plateau. *Tectonophysics*, 399(1–4), 15–37.
- Molnar, P., Brown, E. T., Burchfiel, B. C., Deng, Q., Feng, X., Li, J., Raisbeck, G. M., Shi, J., Wu, Z., Yiou, F., and You, H. (1994). Quaternary climate change and the formation of river terraces across growing anticlines on the north flank of the Tien Shan, China. *J. Geol.*, 102(5), 583–602.
- Mottram, C. M., Kellett, D. A., Barresi, T., Zwingmann, H., Friend, M., Todd, A., and Percival, J. B. (2020). Syncing fault rock clocks: direct comparison of U–Pb carbonate and K–Ar illite fault dating methods. *Geology*, 48(12), 1179–1183.
- Muñoz-López, D., Cruset, D., Vergés, J., Cantarero, I., Benedicto, A., Mangenot, X., Albert, R., Gerdes, A., Beranoaguirre, A., and Travé, A. (2022). Spatio-temporal variation of fluid flow behavior along a fold: the Bóixols-Sant Corneli anticline (Southern Pyrenees) from U–Pb dating and structural, petrographic and geochemical constraints. *Mar. Pet. Geol.*, 143, article no. 105788.
- Müller, W. (2003). Strengthening the link between geochronology, textures and petrology. *Earth Planet. Sci. Lett.*, 206, 237–251.
- Nádor, A., Lantos, M., Tóth-Makk, Á., and Thamó-Bozsó, E. (2003). Milankovitch-scale multi-proxy records from fluvial sediments of the last 2.6 Ma, Pannonian Basin, Hungary. *Quat. Sci. Rev.*, 22(20), 2157–2175.
- Najafi, M., Beamud, E., Ruh, J., Mouthereau, F., Tahmasbi, A., Bernaola, G., Yassaghi, A., Motamedi, H., Sherkati, S., Ghasem Hassan Goodarzi, M., and Vergés, J. (2021). Pliocene growth of the Dowlatabad syncline in Frontal Fars arc: folding propagation across the Zagros Fold Belt, Iran. *Geol. Soc. Am. Bull.*, 133(7–8), 1381–1403.
- Nuriel, P., Craddock, J., Kylander-Clark, A. R., Uysal, I. T., Karabacak, V., Dirik, R. K., Hacker, B. R., and Weinberger, R. (2019). Reactivation history of the North Anatolian fault zone based on calcite age-strain analyses. *Geology*, 47(5), 465–469.
- Nuriel, P., Rosenbaum, G., Zhao, J. X., Feng, Y., Golding, S. D., Villemant, B., and Weinberger, R. (2012). U–Th dating of striated fault planes. *Geology*, 40(7), 647–650.
- Pagel, M., Bonifacie, M., Schneider, D. A., Gautheron, C., Brigaud, B., Calmels, D., Cros, A., Saint-Bezar, B., Landrien, P., Sutcliffe, C., Davis, D., and Chaduteau, C. (2018). Improving paleohydrological and diagenetic reconstructions in calcite veins and breccia of a sedimentary basin by combining $\Delta 47$ temperature, $\delta 18\text{O}_{\text{water}}$ and U–Pb age. *Chem. Geol.*, 481, 1–17.
- Pană, D. I. and van der Pluijm, B. (2015). Orogenic pulses in the Alberta rocky mountains: radiometric dating of major faults and comparison with the regional tectono-stratigraphic record. *Geol. Soc. Am. Bull.*, 127, 480–502.
- Parizot, O., Missenard, Y., Haurine, F., Blaise, T., Barbarand, J., Benedicto, A., and Sarda, P. (2021). When did the Pyrenean shortening end? Insight from U–Pb geochronology of syn-faulting calcite (Corbières area, France). *Terra Nova*, 33, 551–559.
- Parrish, R. R., Parrish, C. M., and Lasalle, S. (2018). Vein calcite dating reveals Pyrenean orogen as cause of Paleogene deformation in southern England. *J. Geol. Soc.*, 175, 425–442.
- Pavlovskaya, E. A., Khudoley, A. K., Ruh, J. B., Moskalenko, A. N., Guillon, M., and Malyshev, S. V. (2022). Tectonic evolution of the northern Verkhoyansk fold-and-thrust belt: insights from palaeostress analysis and U–Pb calcite dating. *Geol. Mag.*, 159, 2132–2156.
- Pazzaglia, F. J. and Brandon, M. T. (2001). A fluvial

- record of long-term steady-state uplift and erosion across the Cascadia forearc high, western Washington State. *Am. J. Sci.*, 301(4–5), 385–431.
- Pevear, D. R. (1999). Illite and hydrocarbon exploration. *Proc. Natl. Acad. Sci. USA*, 96(7), 3440–3446.
- Philippe, Y. (1995). *Rampes latérales et zones de transfert dans les chaînes plissées : géométrie, conditions de formation et pièges structuraux associés*. PhD thesis, Univ. de Savoie, Grenoble. Unpublished, 257 pp.
- Pirouz, M., Avouac, J.-P., Hassanzadeh, J., Kirschvink, J. L., and Bahroudi, A. (2017). Early Neogene foreland of the Zagros, implications for the initial closure of the Neo-Tethys and kinematics of crustal shortening. *Earth Planet. Sci. Lett.*, 477, 168–182.
- Poblet, J., McClay, K., Storti, F., and Munoz, J. A. (1997). Geometry of syntectonic sediments associated with single-layer detachment folds. *J. Struct. Geol.*, 19, 369–381.
- Rahl, J. M., Haines, S. H., and van der Pluijm, B. A. (2011). Links between orogenic wedge deformation and erosional exhumation: evidence from illite age analysis of fault rock and detrital thermochronology of syn-tectonic conglomerates in the Spanish Pyrenees. *Earth Planet. Sci. Lett.*, 307(1–2), 180–190.
- Rasbury, E. T. and Cole, J. M. (2009). Directly dating geologic events: U–Pb dating of carbonates. *Rev. Geophys.*, 47, article no. RG3001.
- Rasbury, E. T., Present, T. M., Northrup, P., Tappero, R. V., Lanzirrotti, A., Cole, J. M., Wooton, K. M., and Hatton, K. (2021). Tools for uranium characterization in carbonate samples: case studies of natural U–Pb geochronology reference materials. *Geochronology*, 3, 103–122.
- Rattez, H. and Veveakis, M. (2020). Weak phases production and heat generation control fault friction during seismic slip. *Nat. Commun.*, 11, article no. 350.
- Reynolds, Jr., R. (1993). *WILDFIRE: A Computer Program for the Calculation of Three-dimensional Powder X-ray Diffraction Patterns for Mica Polymorphs and their Disordered Variations*. R. C. Reynolds, Hanover, NH.
- Riba, O. (1976). Syntectonic unconformities of the Alto Cardener, Spanish Pyrenees: a genetic interpretation. *Sedim. Geol.*, 15, 213–233.
- Ring, U. and Gerdes, A. (2016). Kinematics of the Alpenrhein-Bodensee graben system in the central Alps: oligocene/miocene transtension due to formation of the western Alps arc. *Tectonics*, 35, 1367–1391.
- Rizza, M., Abdrakhmatov, K., Walker, R., Braucher, R., Guillou, V., Carr, A. S., Campbell, G., McKenzie, D., Jackson, J., Aumaître, G., Bourlès, D. L., and Keddadouche, K. (2019). Rate of slip from multiple quaternary dating methods and paleoseismic investigations along the Talas-Fergana Fault: tectonic implications for the Tien Shan range. *Tectonics*, 38(7), 2477–2505.
- Roberts, N. M., Rasbury, E. T., Parrish, R. R., Smith, C. J., Horstwood, M. S., and Condon, D. J. (2017). A calcite reference material for LA-ICP-MS U–Pb geochronology. *G-cubed*, 18(7), 2807–2814.
- Roberts, N. M. and Walker, R. J. (2016). U–Pb geochronology of calcite-mineralized faults: absolute timing of rift-related fault events on the north-east Atlantic margin. *Geology*, 44, 531–534.
- Roberts, N. M., Žák, J., Vacek, F., and Sláma, J. (2021). No more blind dates with calcite: fluid-flow vs. fault-slip along the Očkov thrust, Prague Basin. *Geosci. Front.*, 12(4), article no. 101143.
- Roberts, N. M. W., Drost, K., Horstwood, M. S. A., Condon, D. J., Chew, D., Drake, H., Milodowski, A. E., McLean, N. M., Smye, A. J., Walker, R. J., Haslam, R., Hodson, K., Imber, J., Beaudoin, N., and Lee, J. K. (2020). Laser ablation inductively coupled plasma mass spectrometry (LA-ICP-MS) U–Pb carbonate geochronology: strategies, progress, and limitations. *Geochronology*, 2, 33–61.
- Roberts, N. M. W. and Holdsworth, R. E. (2022). Timescales of faulting through calcite geochronology: a review. *J. Struct. Geol.*, 158, article no. 104578.
- Rockwell, T. K., Keller, E. A., and Dembroff, G. R. (1988). Quaternary rate of folding of the Ventura Avenue anticline, western Transverse Ranges, southern California. *Geol. Soc. Am. Bull.*, 100(6), 850–858.
- Ruh, J. B., Hirt, A. M., Burg, J.-P., and Mohammadi, A. (2014). Forward propagation of the Zagros simply folded belt constrained from magnetostratigraphy of growth strata. *Tectonics*, 33, 1534–1551.
- Saura, E., Vergés, J., Homke, S., Blanc, E., Serra-Kiel, J., Bernaola, G., Casciello, E., Fernandez, N., Romaire, I., Casini, G., Embry, J. C., Sharp, I. R., and Hunt, D. W. (2011). Basin architecture and growth folding of the NW Zagros early foreland basin dur-

- ing the late cretaceous and early tertiary. *J. Geol. Soc.*, 168(1), 235–250.
- Scheiber, T., Viola, G., van der Lelij, R., Margreth, A., and Schönenberger, J. (2019). Microstructurally-constrained versus bulk fault gouge K–Ar dating. *J. Struct. Geol.*, 127, article no. 103868.
- Schneider, C. L., Hummon, C., Yeats, R. S., and Huftile, G. L. (1996). Structural evolution of the northern Los Angeles basin, California, based on growth strata. *Tectonics*, 15(2), 341–355.
- Simoes, M., Avouac, J. P., Chen, Y. G., Singhvi, A. K., Wang, C. Y., Jaiswal, M., Chan, Y. C., and Bernard, S. (2007). Kinematic analysis of the Pakuashan fault tip fold, west central Taiwan: shortening rate and age of folding inception. *J. Geophys. Res. Solid Earth*, 112(B3), article no. B03S14.
- Smeraglia, L., Looser, N., Fabbri, O., Choulet, F., Guillon, M., and Bernasconi, S. M. (2021). U–Pb dating of middle Eocene–Pliocene multiple tectonic pulses in the Alpine foreland. *Solid Earth*, 12(11), 2539–2551.
- Sobel, E. R., Oskin, M., Burbank, D., and Mikolaichuk, A. (2006). Exhumation of basement-cored uplifts: example of the Kyrgyz range quantified with apatite fission track thermochronology. *Tectonics*, 25, article no. TC2008.
- Solum, J. G. and van der Pluijm, B. A. (2007). Reconstructing the Snake River–Hoback River Canyon section of the Wyoming thrust belt through direct dating of clay-rich fault rocks. *Geol. Soc. Am. Spec. Papers*, 433, 183–196.
- Solum, J. G., van der Pluijm, B. A., and Peacor, D. R. (2005). Neocrystallization, fabrics and age of clay minerals from an exposure of the Moab Fault, Utah. *J. Struct. Geol.*, 27(9), 1563–1576.
- Song, Y. and Sim, H. (2021). Illite-Age-Analysis (IAA) for the dating of shallow faults: prerequisites and procedures for improvement. *Minerals*, 11(11), article no. 1162.
- Srodon, J. and Eberl, D. (1984). In Bailey, S., editor, *Micas*, volume 13 of *Mineralogical Society of America Reviews in Mineralogy, Illite*. Mineralogical Society of America.
- Srodon, J. A. N., Clauer, N., and Eberl, D. D. (2002). Interpretation of K–Ar dates of illitic clays from sedimentary rocks aided by modeling. *Am. Mineral.*, 87(11–12), 1528–1535.
- Suppe, J., Chou, G. T., and Hook, S. C. (1992). Rates of folding and faulting determined from growth strata. In McClay, K. R., editor, *Thrust Tectonics*, pages 105–121. Chapman & Hall, Suffolk.
- Tagami, T. (2012). Thermochronological investigation of fault zones. *Tectonophysics*, 538, 67–85.
- Tartaglia, G., Viola, G., van der Lelij, R., Scheiber, T., Ceccato, A., and Schönenberger, J. (2020). “Brittle structural facies” analysis: a diagnostic method to unravel and date multiple slip events of long-lived faults. *Earth Planet. Sci. Lett.*, 545, article no. 116420.
- Tavani, S., Storti, F., Lacombe, O., Corradetti, A., Muñoz, J., and Mazzoli, S. (2015). A review of deformation pattern templates in foreland basin systems and fold-and-thrust belts: implications for the state of stress in the frontal regions of thrust wedges. *Earth-Sci. Rev.*, 141, 82–104.
- Taylor, F. W. and Mann, P. (1991). Late quaternary folding of coral reef terraces, Barbados. *Geology*, 19(2), 103–106.
- Thacker, J. O. and Karlstrom, K. E. (2019). Comment on: U–Pb dating of calcite veins reveals complex stress evolution and thrust sequence in the Bighorn Basin, Wyoming, USA. *Geology*, 47(9), article no. e480.
- Thompson, S. C., Weldon, R. J., Rubin, C. M., Abdrakhmatov, K., Molnar, P., and Berger, G. W. (2002). Late quaternary slip rates across the central Tien Shan, Kyrgyzstan, central Asia. *J. Geophys. Res. Solid Earth*, 107(B9), article no. ETG-7, 7–32.
- Thompson Jobe, J. A., Li, T., Bookhagen, B., Chen, J., and Burbank, D. (2018). Dating growth strata and basin fill by combining $^{26}\text{Al}/^{10}\text{Be}$ burial dating and magnetostratigraphy: constraining active deformation in the Pamir–Tian Shan convergence zone, NW China. *Lithosphere*, 10(6), 806–828.
- Tillberg, M., Drake, H., Zack, T., Kooijman, E., Whitehouse, M. J., and Åström, M. E. (2020). In situ Rb–Sr dating of slickenfibres in deep crystalline basement faults. *Sci. Rep.*, 10(1), 1–13.
- Torgersen, E., Gabrielsen, R. H., Ganerød, M., van der Lelij, R., Schönenberger, J., Nystuen, J. P., and Brask, S. (2022). Repeated brittle reactivations of a pre-existing plastic shear zone: combined K–Ar and ^{40}Ar – ^{39}Ar geochronology of the long-lived (>700 Ma) Himdalen–Ørje deformation zone, SE Norway. *Geol. Mag.*, 159, 2110–2131.
- Torgersen, E., Viola, G., Zwingmann, H., and Harris, C. (2015a). Structural and temporal evolution of a reactivated brittle–ductile fault—Part II: Timing

- of fault initiation and reactivation by K–Ar dating of synkinematic illite/muscovite. *Earth Planet. Sci. Lett.*, 410, 212–224.
- Torgersen, E., Viola, G., Zwingmann, H., and Henderson, I. H. (2015b). Inclined K–Ar illite age spectra in brittle fault gouges: effects of fault reactivation and wallrock contamination. *Terra Nova*, 27(2), 106–113.
- van der Pluijm, B. A., Hall, C. M., Vrolijk, P. J., Pevear, D. R., and Covey, M. C. (2001). The dating of shallow faults in the Earth's crust. *Nature*, 412(6843), 172–175.
- van der Pluijm, B. A., Vrolijk, P. J., Pevear, D. R., Hall, C. M., and Solum, J. (2006). Fault dating in the Canadian rocky mountains: evidence for late Cretaceous and early Eocene orogenic pulses. *Geology*, 34(10), 837–840.
- Velde, B. (1965). Experimental determination of muscovite polymorph stabilities. *Am. Mineral.*, 50, 436–449.
- Velde, B. and Hower, J. (1963). Petrological significance of illite polymorphism in Paleozoic sedimentary rocks. *Am. Mineral.*, 48, 1239–1254.
- Verdel, C., Niemi, N., and Van Der Pluijm, B. A. (2011). Variations in the illite to muscovite transition related to metamorphic conditions and detrital muscovite content: insight from the Paleozoic passive margin of the southwestern United States. *J. Geol.*, 119(4), 419–437.
- Vergés, J., Marzo, M., and Muñoz, J. A. (2002). Growth strata in foreland settings. *Sedim. Geol.*, 146(1–2), 1–9.
- Viola, G., Mancktelow, N. S., Seward, D., Meier, A., and Martin, S. (2003). The Pejo fault system: an example of multiple tectonic activity in the Italian Eastern Alps. *Geol. Soc. Am. Bull.*, 115(5), 515–532.
- Viola, G., Musumeci, G., Mazzarini, F., Tavazzani, L., Curzi, M., Torgersen, E., van der Lelij, R., and Aldega, L. (2022). Structural characterization and K–Ar illite dating of reactivated, complex and heterogeneous fault zones: lessons from the Zuccale Fault, Northern Apennines. *Solid Earth*, 13(8), 1327–1351.
- Viola, G., Scheiber, T., Fredin, O., Zwingmann, H., Margreth, A., and Knies, J. (2016). Deconvoluting complex structural histories archived in brittle fault zones. *Nat. Commun.*, 7(1), 1–10.
- Viola, G., Torgersen, E., Mazzarini, F., Musumeci, G., van der Lelij, R., Schönenberger, J., and Garofalo, P. S. (2018). New constraints on the evolution of the inner Northern Apennines by K–Ar dating of Late Miocene–Early Pliocene compression on the Island of Elba, Italy. *Tectonics*, 37(9), 3229–3243.
- Viola, G., Zwingmann, H., Mattila, J., and Käpyaho, A. (2013). K–Ar illite age constraints on the Proterozoic formation and reactivation history of a brittle fault in Fennoscandia. *Terra Nova*, 25(3), 236–244.
- Vrolijk, P., Pevear, D., Covey, M., and LaRiviere, A. (2018). Fault gouge dating: history and evolution. *Clay Miner.*, 53(3), 305–324.
- Vrolijk, P. and van der Pluijm, B. A. (1999). Clay gouge. *J. Struct. Geol.*, 21(8–9), 1039–1048.
- Wang, Y., Zwingmann, H., Zhou, L., Lo, C.-H., Viola, G., and Hao, J. (2016). Direct dating of folding events by $^{40}\text{Ar}/^{39}\text{Ar}$ analysis of synkinematic muscovite from flexural-slip planes. *J. Struct. Geol.*, 83, 46–59.
- Yamato, P., Kaus, B. J., Mouthereau, F., and Castelltort, S. (2011). Dynamic constraints on the crustal-scale rheology of the Zagros fold belt, Iran. *Geology*, 39, 815–818.
- Ylagan, R. F., Kim, C. S., Pevear, D. R., and Vrolijk, P. J. (2002). Illite polytype quantification for accurate K–Ar age determination. *Am. Mineral.*, 87, 1536–1545.
- Zapata, T. R. and Allmendinger, R. W. (1996). Growth stratal records of instantaneous and progressive limb rotation in the Precordillera thrust belt and Bermejo basin, Argentina. *Tectonics*, 15(5), 1065–1083.
- Zuccari, C., Viola, G., Curzi, M., Aldega, L., and Vignaroli, G. (2022). What steers the “folding to faulting” transition in carbonate-dominated seismic fold-and-thrust belts? New insights from the Eastern Southern Alps (Northern Italy). *J. Struct. Geol.*, 157, article no. 104560.
- Zwingmann, H. and Mancktelow, N. (2004). Timing of Alpine fault gouges. *Earth Planet. Sci. Lett.*, 223(3–4), 415–425.
- Zwingmann, H., Mancktelow, N., Antognini, M., and Lucchini, R. (2010). Dating of shallow faults: new constraints from the AlpTransit tunnel site (Switzerland). *Geology*, 38, 487–490.